

## Current Status and Future Plans for Experiment AD-4 Biological Effectiveness of Antiproton Annihilation

Michael Holzscheiter<sup>1</sup>, Jan Alsner<sup>2</sup>, Angelo Angelopoulos<sup>3</sup>, Niels Bassler<sup>2,4</sup>, Gerd Beyer<sup>5</sup>, John DeMarco<sup>6</sup>, Michael Doser<sup>7</sup>, Dragan Hajdukovic<sup>8</sup>, Oliver Hartley<sup>5</sup>, Adam Hunniford<sup>9</sup>, Kei Iwamoto<sup>6</sup>, Oliver Jäkel<sup>4</sup>, Ioannis Kantemiris<sup>3</sup>, Helge Knudsen<sup>10</sup>, Sandra Kovacevic<sup>8</sup>, Bill McBride<sup>6</sup>, Søren Pape Møller<sup>10</sup>, Robert McCullough<sup>9</sup>, Jens Overgaard<sup>2</sup>, Jørgen Petersen<sup>2</sup>, Osman Ratib<sup>5</sup>, Timothy Solberg<sup>11</sup>, Ulrik Uggerhøj<sup>10</sup>, Sanja Vranjes<sup>12</sup>, and Brad Wouters<sup>13</sup>

<sup>1</sup> University of New Mexico

<sup>2</sup> Aarhus University Hospital

<sup>3</sup> University of Athens

<sup>4</sup> Deutsches Krebsforschungszentrum

<sup>5</sup> Geneva University Hospital

<sup>6</sup> University of California at Los Angeles

<sup>7</sup> CERN

<sup>8</sup> University of Montenegro

<sup>9</sup> Queens University of Belfast

<sup>10</sup> Aarhus University

<sup>11</sup> University of Nebraska Medical Center

<sup>12</sup> Vinca Institute of Nuclear Sciences

<sup>13</sup> University of Maastricht

### Summary

A first round of experiments conducted in 2003 and 2004 at CERN and at TRIUMF have shown a significant enhancement of the biological effective dose ratio (BEDR) for antiprotons compared to protons. The experimental methods and analysis as well as the definition of terms used are described in the 2006 publication in *Radiotherapy & Oncology* (see appendix A). In 2006 the AD-4 collaboration conducted a set of experiments at higher beam energy and therefore deeper penetration into the target. This allowed for the first time the use of a clinically relevant spread-out Bragg peak (SOBP). Early 2007 we performed a set of irradiations using the same methods and materials at GSI with carbon ions giving the same penetration depth and the same SOBP as the antiprotons at CERN. Due to problems with the a priori estimate of dose in the case of antiprotons, a number of data points were rendered. During the 2008 AD-4 Run in week 42 this problem was rectified and a large set of biological data were taken. The remaining missing link to presenting these results in publishable form is a control measurement using a standard Cobalt radiation source and the exact cell lines and preparation routines used in October.

Parallel to the biological measurements with antiprotons in 2007 and 2008 we performed detailed dosimetric studies of the antiproton beam. Using Alanine tablets and ionization chambers to measure the response to the antiproton beam and comparing these results to predictions using different Monte Carlo calculations, we were able to benchmark the FLUKA code package.

As a result of the work in 2007 and 2008 we submitted three papers of which two are accepted and in press (see Appendices B and C). The third paper (on absolute dosimetry using Alanine tablets) is in the final review stage with the referees and we expect acceptance in the very near future.

## II. Introduction:

The overall goal of the AD-4 Experiment is to study the biological effect of antiprotons in order to validate earlier theoretical predictions that antiprotons could produce a yield a better therapeutic ratio for the treatment of well defined tumors. This prediction is based on two observations:

1. The physical dose should be augmented near the end of range due to the additional energy deposited locally when antiprotons annihilate.
2. Some of the additional energy deposited results from low energy heavy ion recoils produced in the annihilation event, which are expected to exhibit a higher biological efficiency.

For this purpose several studies are needed. One is a detailed measurement of the dose deposition of an antiproton beam of a specific energy entering a biological target, which then can be compared to Monte Carlo calculations and can be used to benchmark different available codes. The second piece of information needed is the relative biological effect with respect to a standard radiation type (typically a  $^{60}\text{Co}$  source) along the path of the antiproton beam, preferably for a number of different cell lines extensively used in cancer therapy. Once these two questions are answered one can then use these results as input data for treatment planning tools and develop comparative treatment plans for a specific tumor for antiprotons, carbon ions, and protons. Based on these plans we would then be able to determine specific incidences of cancer where antiprotons could provide a significant benefit to patients.

Since antiproton annihilation also yields a significant component of medium and high-energy secondary particles, which will leave the annihilation vertex, a third, very critical, issue to be studied is the biological effect of this background on cells outside the direct target area.

## III. Biological Measurements:

In October 2006 we performed our first studies of cell survival using a 502 MeV/c antiproton beam from the AD. This beam energy allowed a penetration into our target of approximately 10 cm and much more closely resembled possible therapeutic situations. In addition we used a set of passive degraders to generate a spread-out Bragg peak of 10 mm depth, irradiating a volume of approximately 300 mm<sup>3</sup>. A typical dose-depth profile for both antiprotons is shown in figure 1.

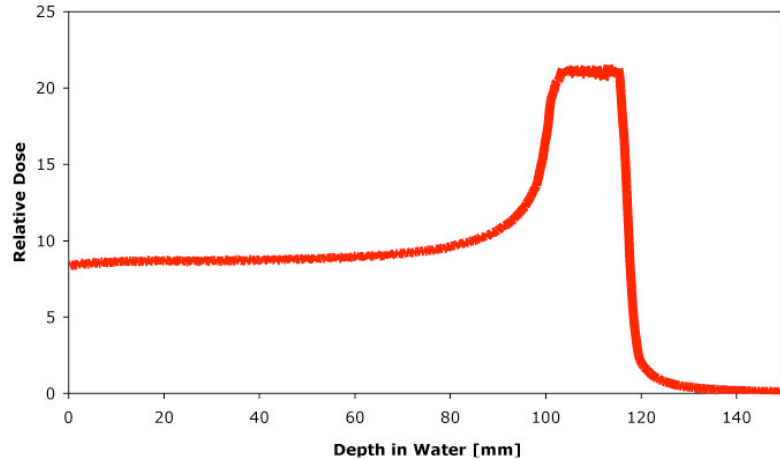


Fig. 1: Typical relative depth dose profile used at CERN for antiprotons obtained from FLUKA.

In 2006 we performed 4 different irradiations with nominal dose values of 0.25, 0.5, 1, and 5 Gy. Due to high uncertainties in estimating the absolute dose only the lowest three dose values yielded useful data, which were presented in the last report (SPSC-2007-020/M-756). For the 2007 run period we had improved our dosimetry capabilities and were able to control the absolute dose delivered to the target to within 10%, allowing us to augment above data sets. We performed irradiations on V79 cells for 6 different dose values. These dose values were selected using FLUKA based on dosimetric information obtained before the irradiation. Control measurements between different badges were performed to assure the stability of the beam delivery system. The raw data obtained are shown in figure 2 below.

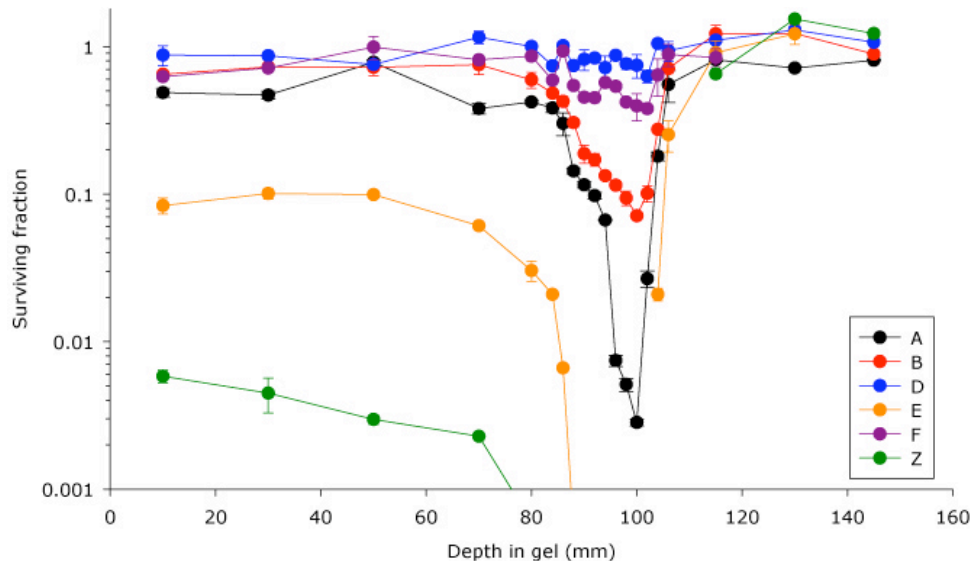


Fig. 2: Survival fraction vs. depth in the target for V79 Chinese Hamster cells irradiated with antiprotons. The dose values for the individual runs were estimated from FLUKA calculations using the number of antiprotons delivered and the radial beam profile obtained from radiochromic film irradiated simultaneously with the cell samples and analyzed after the run. The dose values were A: 2.3 Gy; B: 1.6 Gy; D: 0.5 Gy; E: 6.0 Gy; F: 0.8 Gy; Z: 9.0 Gy.

The above results need to be compared to an experiment using carbon ions conducted in early 2007 at GSI. Here a beam of clinical quality and absolute dosimetry was available and irradiations of 8 samples with plateau dose values between 0.3 and 4.0 Gy were performed. Survival data vs. depth are shown in figure 3.

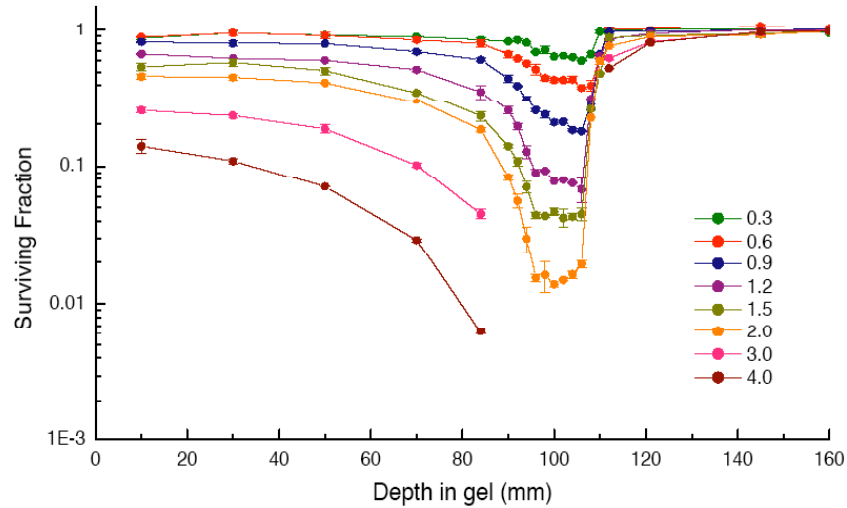


Figure 3: Survival fraction vs. depth in the target for V79 Chinese Hamster cells irradiated with carbon ions

The cell kill in the plateau region is noticeable higher for carbon ions than for antiprotons at similar plateau dose. This is due to the elevated RBE of carbon ions already in the entrance channel. Also noticeable is the earlier and more gradual increase of cell kill for carbon ions compared to antiprotons.

Figure 4 shows the results of our analysis for the carbon ion experiment. Defining the plateau as data points 1 and 2 and the peak as points 9 – 14 of the depth survival curve we can plot survival vs. absolute dose for peak and plateau. In addition we plot survival vs. dose for a reference X-ray source with low LET and RBE of 1. Using a survival rate of 10% we extract the  $RBE_{0.1}$  for carbon ions as 1.38 in the plateau and 2.17 in the peak.

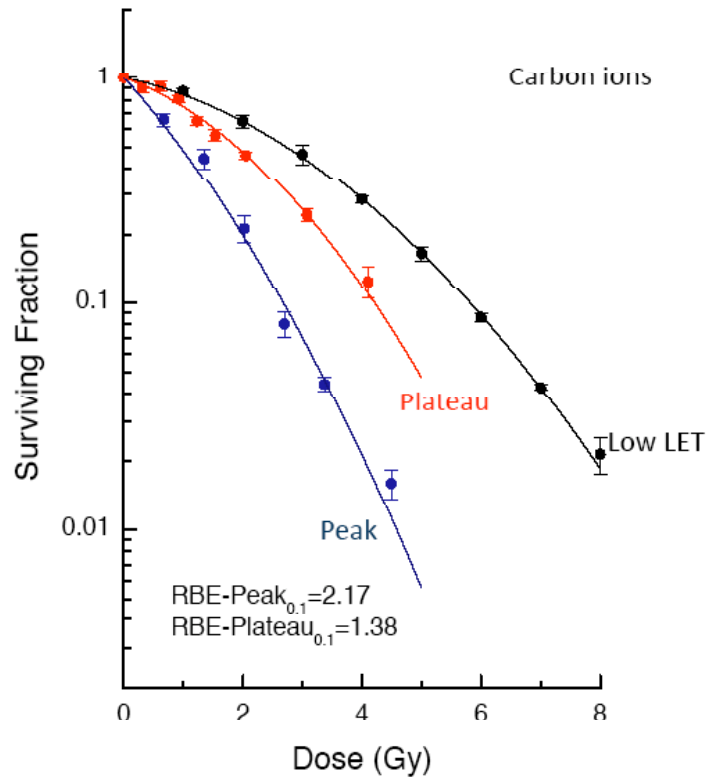


Figure 4: Survival fraction vs. absolute for V79 Chinese Hamster cells irradiated with carbon ions. By comparing the dose needed to achieve a survival of 10% using low LET X-rays to the dose needed when using carbon ions we extract a relative biological efficiency of 1.38 in the plateau and 2.17 in the peak.

In order to perform the same analysis for antiprotons we are currently still lacking a control measurement using a standard  $^{60}\text{Co}$  radiation source for the exact cell preparation used in October 2008. Experience has shown that significant differences in response to low LET radiation must be expected for different batches of the same cell line or when a slightly different preparation of the gelatin is used. As we were forced to move the cell preparation and analysis work from the University of Maastricht to the University Hospital of Aarhus we cannot fully rely on earlier control measurements obtained in 2006.

To illustrate this point we show in figure 4 a preliminary analysis for the relative biological effectiveness of antiprotons based on previous control measurements.

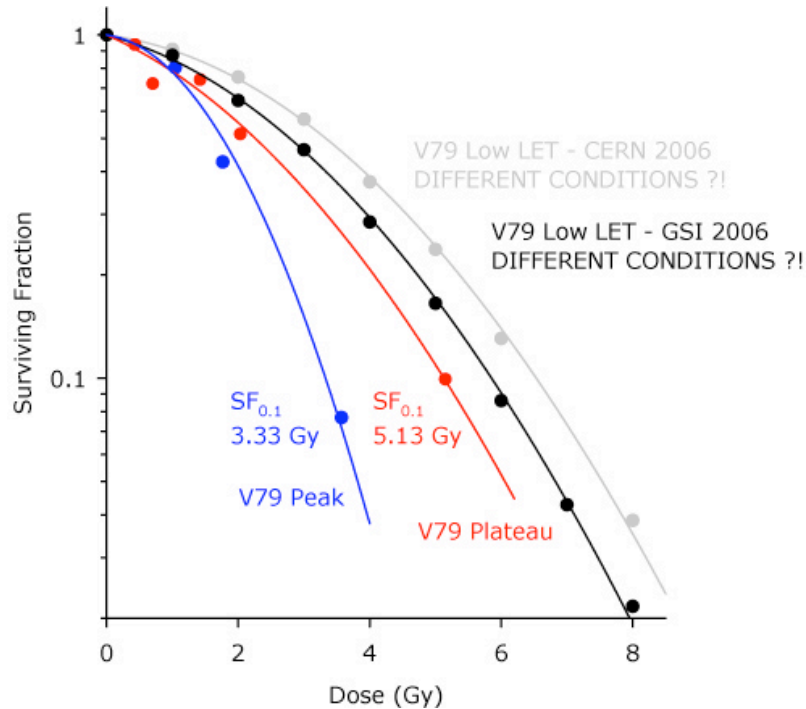


Figure 4: Surviving fraction for V79 Chinese Hamster Cells irradiated with antiprotons plotted vs. dose for peak and plateau. A biological endpoint of 10% cell survival is reached for 3.33 Gy in the peak and for 5.13 Gy in the plateau. Peak and Plateau RBE vary between 1.77 and 1.95 for the peak and 1.15 and 1.27 in the plateau, depending on the choice of reference radiation. As the reference irradiations were done under different conditions a repeat measurement with  $^{60}\text{Co}$  is needed to narrow down these ranges.

Dose values needed to achieve a biological endpoint of 10% cell survival was found to be 3.33 Gy and 5.13 Gy in the peak and plateau respectively. For the previous control samples the dose to achieve the same endpoint varied between 5.9 and 6.5 Gy and a final control measurement using the exact same cell preparation is needed to finalize these results.

In addition to completing the studies with V79 Chinese Hamster cells we continued our studies using human cells (Type FaDuDD) started in 2006 with the goal to identify specific genetic expressions as a result of the irradiation. The 2006 studies were intended as an initial test if specific genetic expressions known in cancer therapy can be observed and as this was the case, we mounted a more systematic study in 2007. 10 samples with FaDuDD cells embedded in the same gel as used for the V79 cells were irradiated with antiprotons at plateau doses between 0.75 Gy and 15 Gy. Samples of these irradiations will in addition to genetic expression studies also be analyzed for survival.

#### IV. Dosimetry Studies:

To interpret a measured response of a biological system exposed to a beam of hadrons in terms of dose deposition, knowledge of the Relative Biological Effectiveness (RBE) for the particular beam of particles is necessary. Similarly, for a radiation detector the

relative effectiveness (RE) is relating the observed detector response with dose deposition.

Attempts to measure the RBE directly in the peak region of an antiproton beam so far have been problematic, since dosimetry of the antiproton depth dose curve is difficult due to the unknown dosimeter response. Ionization chambers behave non-linear due to volume recombination arising from the pulsed nature of the antiproton beam available at CERN. Measurements using Boag's theorem correcting for recombination effects have been performed during the October 2006. The results of these studies have now been finalized and a publication has been accepted and is in press. (See appendix B).

Our earlier measurements with Alanine detectors were augmented this year by additional measurements and compared to the results of simulations using the particle energy spectrum calculated by FLUKA and the track structure model of Hansen et Olsen for conversion of calculated dose into response. Good agreement was observed between the measured and calculated relative effectiveness although a slight underestimation of the calculated values in the Bragg peak remains unexplained. The model prediction of response of alanine towards heavy charged particles encourages future use of the alanine detectors for dosimetry of mixed radiation fields. A paper on these studies has been submitted to NIM B and has received positive reviews by the referees. A final version with some changes and corrections requested by the referees has been sent to the editor and final acceptance is expected very soon (see appendix C for the draft of this paper as submitted).

## **V. Future Plans:**

Depending final analysis of the data collected in 2008 we will define a scientific program for 2008. Aside from augmenting existing data on V79 cells, if necessary, and possible repeat experiments on the FaDuDD studies, we are discussing a number of approaches to the third question raised in the introduction, the peripheral damage to cells outside the direct beam. Again, our approach will be based on computer calculations with a minimal but crucial set of experimental tests for benchmarking.

As for any measurements careful initial dosimetry studies are needed. We plan to develop a program to beneficially use 1 week (7 days) of beam time performing several independent measurements. The exact schedule for the requested beam time will need to be decided within the collaboration to assure availability of laboratory space and personnel, but currently we favor again the time period of late October, early November.

In order to impact the other experiments as minimal as possible we request to be granted the last week of running time at the AD as last year. With the biological preparations necessary and considering the limited survival time of the samples once the cells have been harvested and embedded in gelatin, a precise schedule must be established early on. The actual irradiation time can then be adjusted by a few days within the week by waiting until the beam development is completed and dosimetry has been fully established before preparing the actual samples from cell cultures started a few weeks beforehand.

**VI. Additions to the AD-4 Collaboration:**

As of December 2007 a new Memorandum of Understanding between CERN and the AD-4 collaboration has been executed by all current parties. Since then two new institutions have joined the collaboration, the Queen's University of Belfast, represented by Prof. Robert McCullough, and the University of Athens, represented by Prof. Angelo Angelopoulos. Amendments to the MOU reflecting these additions are currently being drafted by the CERN Legal Service. A current list of institutions and members is given in appendix D.



Appendix A:  
Radiotherapy and Oncology 2008, in press

Original article

Antiproton radiotherapy

Niels Bassler<sup>a,b,\*</sup>, Jan Alsner<sup>a</sup>, Gerd Beyer<sup>c</sup>, John J. DeMarco<sup>d</sup>, Michael Doser<sup>e</sup>,  
Dragan Hajdukovic<sup>f</sup>, Oliver Hartley<sup>c</sup>, Keisuke S. Iwamoto<sup>d</sup>, Oliver Jäkel<sup>b</sup>,  
Helge V. Knudsen<sup>g</sup>, Sandra Kovacevic<sup>f</sup>, Søren Pape Møller<sup>h</sup>, Jens Overgaard<sup>a</sup>,  
Jørgen B. Petersen<sup>i</sup>, Timothy D. Solberg<sup>j</sup>, Brita S. Sørensen<sup>a</sup>, Sanja Vranjes<sup>k</sup>,  
Bradly G. Wouters<sup>l</sup>, Michael H. Holzscheiter<sup>m</sup>

<sup>a</sup>Department of Experimental Clinical Oncology, Aarhus University Hospital, Aarhus, Denmark,

<sup>b</sup>Deutsches Krebsforschungszentrum, Heidelberg, Germany, <sup>c</sup>Hospital Universitaire de Geneve, Geneva, Switzerland,  
<sup>d</sup>David Geffen School of Medicine, UCLA, Los Angeles, CA, USA, <sup>e</sup>CERN, Geneva, Switzerland, <sup>f</sup>University of Montenegro,  
Podgorica, Montenegro, <sup>g</sup>Department of Physics and Astronomy, <sup>h</sup>ISA, University of Aarhus, Denmark,

<sup>i</sup>Department of Medical Physics, Aarhus University Hospital, Aarhus, Denmark, <sup>j</sup>University of Nebraska Medical Center,  
Omaha, NE, USA, <sup>k</sup>VINCA Institute for Nuclear Sciences, Belgrade, Serbia, <sup>l</sup>University of Maastricht, Res.  
Institute Growth and Development, The Netherlands, <sup>m</sup>University of New Mexico, Albuquerque, NM, USA

Abstract

Antiprotons are interesting as a possible future modality in radiation therapy for the following reasons: When fast antiprotons penetrate matter, protons and antiprotons have near identical stopping powers and exhibit equal radiobiology well before the Bragg-peak. But when the antiprotons come to rest at the Bragg-peak, they annihilate, releasing almost 2 GeV per antiproton–proton annihilation. Most of this energy is carried away by energetic pions, but the Bragg-peak of the antiprotons is still locally augmented with ~20–30 MeV per antiproton. Apart from the gain in physical dose, an increased relative biological effect also has been observed, which can be explained by the fact that some of the secondary particles from the antiproton annihilation exhibit high-LET properties. Finally, the weakly interacting energetic pions, which are leaving the target volume, may provide a real time feedback on the exact location of the annihilation peak.

We have performed dosimetry experiments and investigated the radiobiological properties using the antiproton beam available at CERN, Geneva. Dosimetry experiments were carried out with ionization chambers, alanine pellets and radiochromic film. Radiobiological experiments were done with V79 WNRE Chinese hamster cells. The radiobiological experiments were repeated with protons and carbon ions at TRIUMF and GSI, respectively, for comparison. Several Monte Carlo particle transport codes were investigated and compared with our experimental data obtained at CERN. The code that matched our data best was used to generate a set of depth dose data at several energies, including secondary particle-energy spectra. This can be used as base data for a treatment planning software such as TRiP.

Our findings from the CERN experiments indicate that the biological effect of antiprotons in the plateau region may be reduced by a factor of 4 for the same biological target dose in a spread-out Bragg-peak, when comparing with protons.

The extension of TRiP to handle antiproton beams is currently in progress. This will enable us to perform planning studies, where the potential clinical consequences can be examined, and compared to those of other beam modalities such as protons, carbon ions, or IMRT photons.

© 2007 Published by Elsevier Ireland Ltd. Radiotherapy and Oncology xx (2007) xxx–xxx.

Keywords: Antiproton; RBE; Particle irradiation

Antiproton therapy might sound like science fiction but in fact, antiproton therapy may well be clinically beneficial for selected cases and could perhaps be economically feasible if performed in the context of a major facility producing antiproton beams for fundamental science research. Gray and Kalogeropoulos first suggested radiation therapy with antiprotons in 1984 based on Monte Carlo calculation of a

significant enhancement of physical dose in the Bragg-peak [1]. Sullivan shortly afterwards measured an enhancement of the peak-to-plateau ratio of physical dose deposition by antiprotons in polyethylene by a factor of 2 compared to protons [2]. Since reducing normal tissue morbidity is one of the main goals of radiotherapy, beam modalities such as IMRT, proton beam therapy and carbon ion beams have

55 been investigated during the last decades and have been  
56 successfully implemented in clinical use [3–7]. Other parti-  
57 cles, such as fast neutrons and pions, were applied in radi-  
58 ation therapy, but proved to be less successful in the clinical  
59 settings [8,9]. Antiprotons deserve closer investigation since  
60 they exhibit the precision in dose delivery of a charged parti-  
61 cle and confine the contribution of high linear energy  
62 transfer (LET) to the Bragg-peak.

## 63 Annihilation physics

64 When fast antiprotons penetrate matter, they have the  
65 same stopping power as protons. The amount of primary  
66 particle loss is only slightly larger for antiprotons when com-  
67 pared with protons, and is less than that of carbon ions [10].

68 As the antiproton comes to rest, it will preferably be cap-  
69 tured by a high-Z nucleus. For a polystyrene target ~99% of  
70 the antiprotons will therefore annihilate on a carbon nucleus,  
71 whereas the rest will annihilate with a hydrogen nucleus [11].  
72 When captured by the target atoms, the antiproton will  
73 immediately spiral towards the nucleus and annihilate on its  
74 surface. This annihilation process releases 1.88 GeV corre-  
75 sponding to twice the rest-mass of the proton and the energy  
76 release is converted on average into 4 or 5 pions [12,13]. The  
77 pions created are  $\pi^+$  and  $\pi^-$  particles, as well as  $\pi^0$ . The  $\pi^0$  mes-  
78 on is highly unstable and decays instantaneously into high en-  
79 ergy gamma-rays with roughly 70–300 MeV [12]. Due to the  
80 solid angle covered by the nucleus, 1 or 2 of the charged pions  
81 are most likely penetrating the nucleus inducing an intra-nu-  
82 clear cascade, causing the nucleus to break into fragments  
83 [14–16]. Charged fragments have a very short range in the  
84 target and will deposit their kinetic energy in the immediate  
85 vicinity of the annihilation vertex. Also, we expect that some  
86 of these fragments will exhibit a high-LET and are responsible  
87 for an increase in biological effectiveness of antiproton anni-  
88 hilation compared to protons stopping in the target. Antipro-  
89 tons annihilating on particles heavier than protons will also  
90 produce neutrons which will have a larger range and will lead  
91 to a certain level of background radiation. This needs to be  
92 studied carefully in the context of validating antiprotons for  
93 radiotherapy applications.

94 The total energy deposited locally by these particles has  
95 been estimated by Gray and Kalogeropoulos using Monte  
96 Carlo calculations [1] to be 30 MeV per antiproton, which  
97 has been confirmed experimentally by Sullivan [2] who used  
98 a continuous beam of antiprotons from the Low Energy Anti-  
99 proton Ring (LEAR) at CERN and standard ionization cham-  
100 bers. This energy represents an increase of the physical  
101 dose deposition in the Bragg-peak by roughly a factor of 2,  
102 when compared to protons. In addition to this augmentation  
103 of the physical dose the secondary particles also cause the  
104 antiproton beam to have different radiobiological proper-  
105 ties in the peak region.

## 106 Antiproton production

107 Currently, only few laboratories in the world produce  
108 antiparticles, and only at CERN, located near Geneva, a

beam of antiprotons at clinical relevant energies is avail- 109  
able. Antiprotons are produced from a 26 GeV proton beam, 110  
which is being dumped into a target. The peak production 111  
occurs at an antiproton energy of 3.6 GeV. Antiprotons are 112  
collected at this production energy in the antiproton decel- 113  
erator (AD) ring, decelerated to lower energies, and cooled 114  
using stochastic cooling as well as electron cooling to de- 115  
crease beam emittance. To date we have used both a 116  
47 MeV and a 126 MeV antiproton beam, which have a range 117  
of approximately 2 or 11 cm in a water phantom, respec- 118  
tively. Every 90 s around  $3 \times 10^7$  antiprotons are delivered 119  
to our experiment, which corresponds to a dose in the pla- 120  
teau region of 30 mGy at  $\sigma = 4$  mm of the Gaussian shaped 121  
beam at 126 MeV. These antiprotons exit the accelerator 122  
vacuum through a 15  $\mu$ m titanium window and pass several 123  
non-destructive beam monitors before entering the biolog- 124  
ical target. A fast current transformer gives the total charge 125  
extracted from the accelerator and a combination of a thin 126  
scintillator and a CCD camera can be used to monitor the 127  
beam position and profile. The antiproton beam focus can 128  
be changed, depending on the experimental requirements, 129  
between  $\sigma = 4$  mm and  $\sigma = 15$  mm. A future antiproton pro- 130  
duction facility for experimental physics is planned at the 131  
Gesellschaft für Schwerionenforschung (GSI) in Darmstadt 132  
and will offer significantly higher beam intensities. 133

## Radiobiology

In 2006 we published an article concerning the radiobiol- 134  
ogy of a 47 MeV antiproton beam, describing the initial 135  
experiments carried out at CERN in 2003 and 2004 [17]. 136  
RBE determination was at that time not possible, since we 137  
could not assess the absolute physical dose for the pulsed 138  
antiproton beam. Instead the Biological Effective Dose Ratio 139  
(BEDR) term was conceived. Recently we have initiated a 140  
new set of measurements at higher energy at CERN and at 141  
GSI to compare the biological effects of antiprotons and 142  
carbon ions using identical experimental conditions. The en- 143  
ergy used of 126 MeV provides a better separation of the 144  
peak from the plateau region and also enables us to produce 145  
a clinically relevant spread-out Bragg peak (SOBP). After 146  
careful dosimetry studies (see next section), we are now 147  
able to adequately assess the absolute physical dose in 148  
the peak region of the pulsed antiproton beam. This will en- 149  
able us to directly determine the RBE in the peak region in 150  
future experiments, which then can be used as an input 151  
parameter for computer models used for treatment 152  
planning. 153  
154

## Dosimetry

Monte Carlo simulations with FLUKA 2006.3 [18,19] of a 155  
pristine beam of antiprotons are shown in Fig. 1. Here a 156  
 $5 \times 5$  cm square field of 502 MeV/c (126 MeV) antiprotons 157  
on a water target was simulated. The dose was scored along 158  
the central beam axis in circular disks with a diameter of 159  
2 cm in 0.5 mm steps. The beam momentum spread was 160  
 $\Delta p/p = 5 \times 10^{-4}$  and the divergence was set to 5 mrad, 161  
162

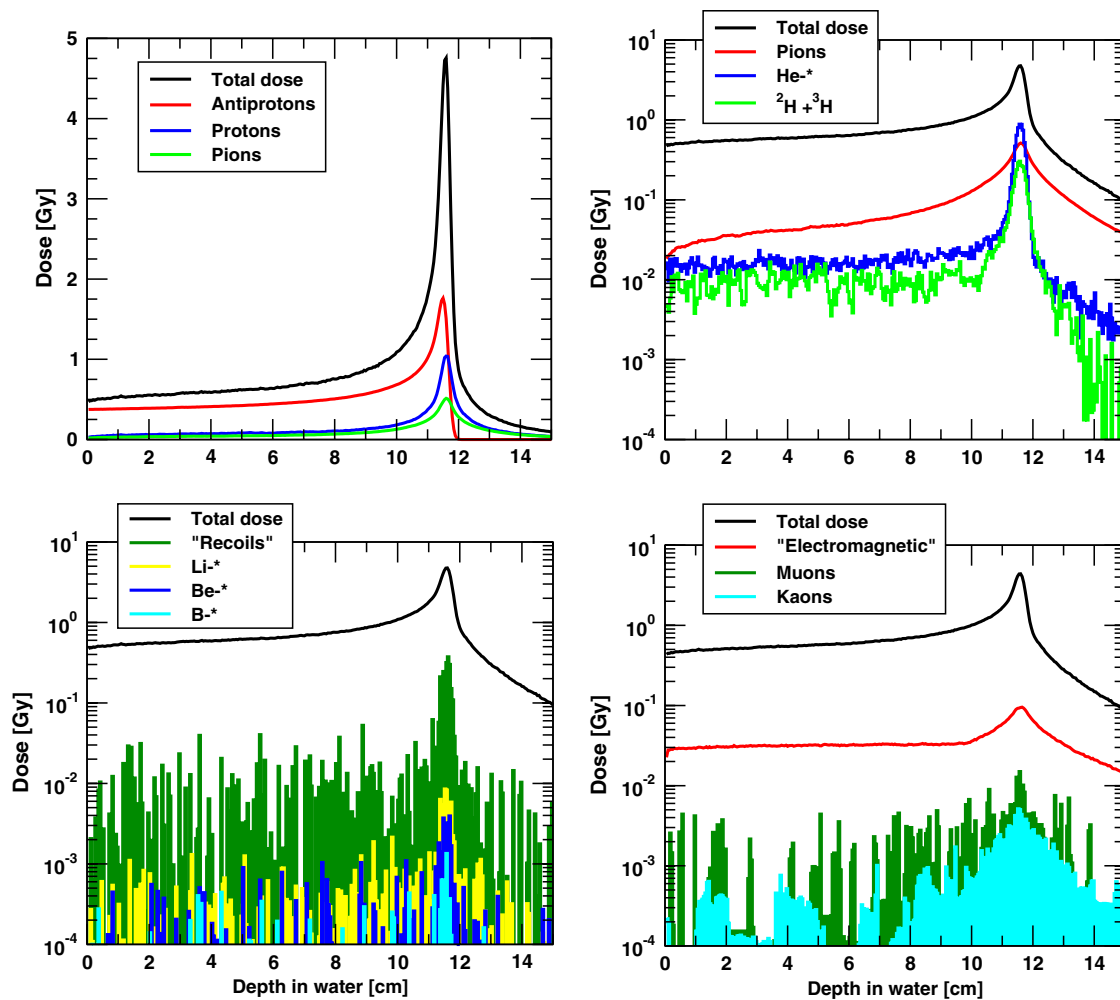


Fig. 1. FLUKA simulation of the depth dose distribution of a square 5×5 cm 126 MeV antiproton field, scaled to 10<sup>10</sup> antiprotons. The dose was averaged over a central cylindrical region with a diameter of 2 cm in steps of 0.5 mm.

163 mimicking the parameters of the beam at CERN. The FLUKA  
164 statistics were 500.000 simulated antiprotons, but the dose  
165 plotted here is scaled to 10<sup>10</sup> antiprotons. Neutrons do not  
166 contribute directly to dose, as these particles are indirectly  
167 ionizing. They generate recoils which are further trans-  
168 ported by FLUKA, if the energy is sufficiently high. Dose  
169 from electrons and positrons generated by photons is con-  
170 tained in the curve labelled "Electromagnetic". The curve  
171 labelled "Recoils" represents dose contributions from  
172 unspecified fragments with low energy (order of keV) which  
173 are not transported. They make up roughly 8% of the total  
174 dose near the annihilation peak. The asterisk in e.g.  
175Q4 "Li-<sup>\*</sup>" refers to all isotopes of Lithium (see Fig. 2).

176 Fig. 1 thus gives an overview of the contributions to the  
177 total dose. The primary antiproton beam (which, by the  
178 way, is almost identical to the depth dose curve of a primary  
179 proton beam) deposits most dose, followed by contributions  
180 from secondary protons, pions, EM-transport and helium nu-  
181 clei. The remaining contributions are significantly less, and  
182 have been plotted on a logarithmic y-axis, else they were  
183 indistinguishable. The secondary particles are mainly cre-  
184 ated at the end of flight, and then emitted isotropically,  
185 which explains the symmetry of the curves at the annihila-

186 tion vertex. Also, interesting enough, the dose contribution  
187 by transported fragments heavier than helium is in the same  
188 order as the dose contributions from muons<sup>1</sup> and the rather  
189 exotic kaons<sup>2</sup>.

190 Dosimetry of an antiproton beam is not trivial due to the  
191 mixed particle spectrum of the secondary particles from  
192 antiproton annihilation. Most, if not all, solid state detec-  
193 tors respond non-linear when subjected to high-LET ionizing  
194 radiation. Often the response depends on energy and charge  
195 of the particle, and usually the behaviour of such detectors  
196 requires a detector model that describes the performance  
197 in mixed particle radiation fields. Initially, alanine detec-  
198 tors, thermoluminescent devices (TLDs), and radiochromic  
199 films were applied in the beam. We found that alanine  
200 detectors [20,21] could be used as an absolute dosimeter  
201 in the plateau region, and to some extent in the mixed par-  
202 ticle environment around the annihilation peak. A model for  
203 the response of the alanine detector in various mono-ener-  
204 getic fields was used in conjunction with Monte Carlo simu-  
205 lations of the particle-energy spectrum in the peak. The

<sup>1</sup> From pion decay.

<sup>2</sup> A few Σ-particles were also encountered during the simulations.

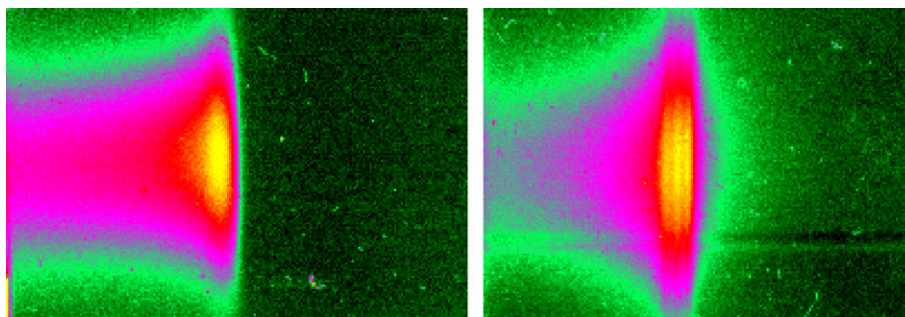


Fig. 2. Measured radiochromic film response for protons (left) and antiprotons (right) at 47 MeV. Both beams were degraded to spread-out the peak.

206 response of alanine to the antiproton beam thus calculated  
207 was in good agreement with the measured response. This  
208 work is subject of a forthcoming publication [22].

209 Apart from alanine detectors, we found that dosimetry  
210 with TLDs is not recommendable due to the lack of ade-  
211 quate LET models and standardised handling procedures of  
212 the detectors, which compromised the reproducibility of  
213 the response in particle fields [23]. Radiochromic films were  
214 until now primarily used for determining the width of the  
215 beam, as well as the position of the annihilation peak, but  
216 not for dosimetry, again due to the lack of models which  
217 can translate the response into dose for mixed particle  
218Q5 spectra. Still, Fig. ? shows effectfully the key differences  
219Q1 between a proton and antiproton beam: here two slanted  
220 radiochromic films were exposed to a Gaussian shaped beam  
221 of protons and antiprotons, respectively, entering from the  
222 left. The beam was spread-out to cover a few mm in the tar-  
223 get region. The colour scale is normalized to match both the  
224 background and peak dose levels. Clearly, the penumbra  
225 due to secondary particles being emitted from the antipro-  
226 ton annihilation can be seen. Secondly, for iso-response in  
227 the peak region, the response in the entry region for the  
228 antiprotons is significantly less pronounced.

229 Relative dosimetry was done with a transmission ioniza-  
230 tion chamber (Advanced Roos Chamber from PTW Freiburg).  
231 Absolute dosimetry for the biology experiment using the  
232 ionization chamber alone was not possible, since the  
233 40 mm diameter of the Advanced Roos Chamber was much  
234 larger than the  $\sim 10$  mm FWHM<sup>3</sup> of the antiproton beam.  
235 Small beam misalignment and changes in FWHM, which seri-  
236 ously impact the dose delivered to the test sample, cannot  
237 be detected by the ionization chamber. Instead, the ioniza-  
238 tion chamber was used for relative dosimetry only. Due to  
239 the pulsed structure of the antiproton spills (one 300 ns spill  
240 every 90 s), it is necessary to compensate for ionic recombi-  
241 nation effects [24,25]. The results of the ionization cham-  
242 ber measurements were compared with the Monte Carlo  
243 particle transport programs SHIELD-HIT v. 2.2 by Sobolevsky  
244 et al. [26] and FLUKA 2006.3. FLUKA proved to be in excel-  
245 lent agreement with our relative ionization chamber mea-  
246 surements, which is shown in Fig. 3, and therefore FLUKA

<sup>3</sup> The FWHM is selected to be sufficiently large to give a reasonably homogeneous dose across the sample tube (which had a diameter of  $\sim 6.5$  mm), while still being small enough in order to use as much as possible of the antiproton beam.

247 was chosen to build the input data needed for the treatment  
248 planning software TRiP [27,28]. A paper concerning these  
249 findings is in preparation [29].

## Treatment planning 250

251 The scarcity of antiprotons (we typically have access to  
252 the antiproton beam at CERN for just one week per year)  
253 dictates that we concentrate our measurements on produc-  
254 ing the necessary database to validate our Monte Carlo  
255 codes. Then we use these codes to generate the set of input  
256 data needed for a biological treatment planning system to  
257 generate a dose plan for a virtual treatment with antipro-  
258 tons that can be compared with a treatment plan calculated  
259 for protons, carbon ions, or other modalities. To date we  
260 have used TRiP to model physical dose distributions based  
261 on the depth dose base curve for antiprotons generated with  
262 FLUKA and compared this to a physical dose distribution for  
263 a carbon ion beam.

264 Fig. 4 is comparing a carbon ion treatment plan (left)  
265 with an antiproton plan (right). The plan is only optimized  
266 for physical dose at this time. Comparing these plans, one  
267 can see that the dose in the entry region is reduced,  
268 whereas the lateral penumbra is slightly more pronounced  
269 for antiprotons. It is still too early to derive conclusions  
270 from this, since the radiobiology optimization is still under  
271 development for antiprotons, and the RBE is expected to  
272 vary significantly along the depth dose curve for antipro-  
273 tons. TRiP already uses the Local Effect Model (LEM) [30–  
274 32] for optimizing the biological dose for carbon ion beams.  
275 To optimize the treatment plan for biological dose for anti-  
276 protons, the complete particle-energy spectrum is needed  
277 for LEM to model the RBE. We have generated such spectra  
278 using FLUKA and are currently implementing these in our  
279 calculations. This will enable us to study a variety of clinical  
280 situations in order to identify those cases where antiproton  
281 therapy may offer improvements over existing particle  
282 beam modalities.

## Conclusion 283

284 So far the arguments for and against antiproton radio-  
285 therapy have been mostly quantitatively. Biological experi-



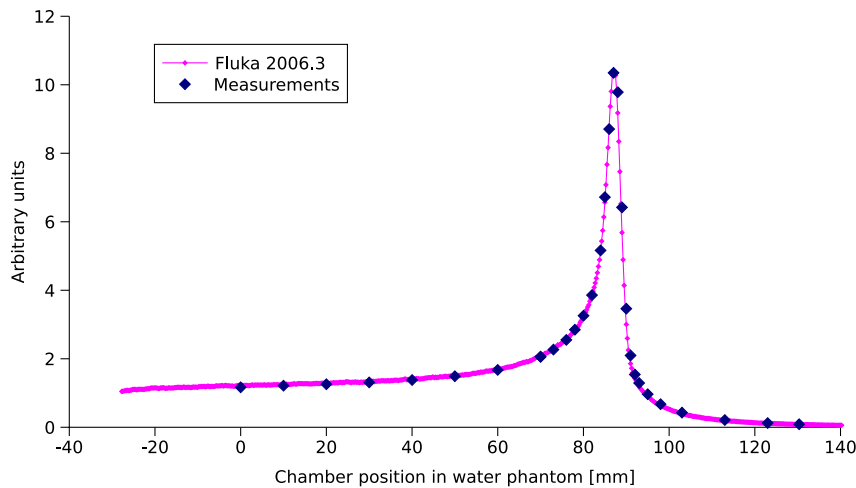


Fig. 3. FLUKA 2006.3 calculated relative dose compared with CERN ionization chamber measurements.

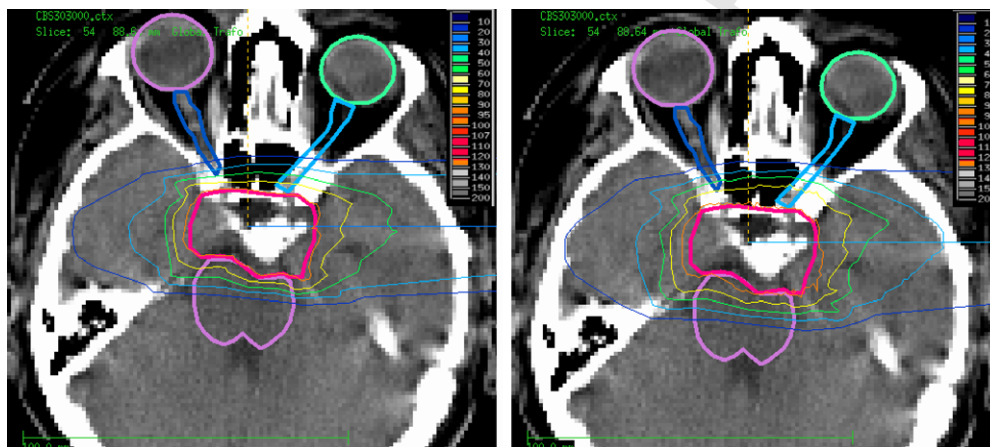


Fig. 4. Physical dose distributions for a single field of carbon ions (left) and antiprotons (right). For antiprotons the entrance dose is noticeably reduced while the lateral penumbra is slightly increased. These calculations do not include any biological effects.

286 ments performed by the AD-4/ACE collaboration at CERN  
287 have shown an enhanced biological effect of 4 in the peak  
288 region for antiprotons compared with protons for the same  
289 entrance dose. Careful antiproton dosimetry experiments  
290 and tests of various Monte Carlo codes have resulted in reli-  
291 able computer simulations of clinical antiproton beam dose  
292 distributions. Combined with the data from the cell survival  
293 experiments the RBE can be calculated in future experi-  
294 ments and can then be implemented in biological treatment  
295 planning systems.

296 The expected possible advantage of antiproton therapy  
297 over other advanced modalities like combined IMRT/IMPT  
298 (protons)/IMPT (carbon ions) is still to be examined in treat-  
299 ment planning studies. One advantage of antiprotons is low-  
300 LET in the plateau (and thereby low alpha/beta ratio for  
301 late responding normal tissue) combined with high-LET, high  
302 RBE and low OER in the peak region for small targets. This  
303 suggests that antiproton therapy could be superior for small  
304 radioresistant targets surrounded by highly radiosensitive  
305 critical normal tissue. This could obviously be re-treatment  
306 of local failures in previously irradiated organs and tumours  
307 like chordomas or chondrosarcomas located between the

308 optical pathways and close to the optic chiasm. Other antic-  
309 ipated uses are boost to hypoxic areas where IMRT and IMPT  
310 (protons and carbon) probably could not give the same BED  
311 conformity as fractionated antiproton therapy; this is again  
312 especially relevant in tumours surrounded by critical normal  
313 structures like hypoxic components in paranasal squamous  
314 cell carcinoma.

**Acknowledgements**

315 The Danish Cancer Society and the ICE Center under the Danish  
316 Natural Science Research Council partially supported this project  
317 with a grant. We very much appreciate the diligent efforts by the  
318 AD operations team to deliver the antiproton beam at CERN and  
319 to develop the new extraction scheme to provide the 126 MeV beam  
320 energy.  
321

\* Corresponding author. Niels Bassler, Deutsches Krebsforsch-  
322 ungszentrum, E0409, Im Neuenheimer Feld 280, 69120 Heidel-  
323 berg, Germany. E-mail address: n.bassler@dkfz.de  
324  
325

Received 24 September 2007; received in revised form 13 November  
2007; accepted 28 November 2007

References

329 [1] Gray L, Kalogeropoulos TE. Possible biomedical applications of  
330 antiproton beams: focused radiation transfer. *Radiat Res*  
331 1984;246–52.

332 [2] Sullivan AH. A measurement of the local energy deposition by  
333 antiprotons coming to rest in tissue-like material. *Phys Med*  
334 *Biol* 1985;30:1297–303.

335 [3] Goitein Michael, Goitein Gudrun. Swedish protons. *Acta*  
336 *Oncologica* 2005;44:793–7.

337 [4] Olsen Dag Rune, Bruland Øjvind S, Frykholm Gunilla, Norderh-  
338 aug Inger Natvig. Proton therapy – A systematic review of  
339 clinical effectiveness. *Radiother Oncol* 2007;83:123–32.

340 [5] Jäkel O, Schulz-Ertner D, Karger CP, Nikoghosyan A, Debus J.  
341 Heavy ion therapy: status and perspectives. *Technol Cancer*  
342 *Res Treat* 2003;2:377–87.

343 [6] Schulz-Ertner Daniela, Jäkel Oliver, Schlegel Wolfgang. Radi-  
344 ation therapy with charged particles. *Semin Radiat Oncol*  
345 2006;16:249–59.

346 [7] Schulz-Ertner Daniela, Tsujii Hirohiko. Particle radiation ther-  
347 apy using proton and heavier ion beams. *J Clin Oncol*  
348 2007;25:953–64.

349 [8] Budach V. The role of fast neutrons in radiooncology – A  
350 critical appraisal. *Strahlenther Onkol* 1991;167:677–92.

351 [9] Wisser L. Pion treatment of prostate carcinoma at Paul  
352 Scherrer Institute (formerly Swiss Institute for Nuclear  
353 Research (SIN)) from 1983 to 1992. *Cancer Radiothérapie*  
354 2004;8:88–94.

355 [10] Bassler N, Holzscheiter M, Knudsen H, The AD4/ACE Collabo-  
356 ration. Cancer therapy with antiprotons. In: Dieter Grzonka,  
357 Rafał Czyżykiewicz, Walter Oelert, Tomasz Rożek, Peter  
358 Winter, editors. *Low Energy Antiproton Physics-LEAP '05*, vol.  
359 CP796 of AIP Conference Proceedings. American Institute of  
360 Physics, 2005; pp. 423–430.

361 [11] Ponomarev LI. Molecular structure effects on atomic and  
362 nuclea capture of mesons. *Annu Rev Nucl Sci* 1973:395–430.

363 [12] Agnew Jr Lewis E, Elioff Tom, Fowler William B, Lander  
364 Richard L, Powell Wilson M, Segrè Emilio, et al. Antiproton  
365 interactions in hydrogen and carbon below 200 MeV. *Phys Rev*  
366 1960:1371–91.

367 [13] Inokuti M. Interactions of antiprotons with atoms and mole-  
368 cules. *Nucl Tracks Radiat Meas* 1989;16:115–23.

369 [14] Cugnon J, Wycech S, Jastrzębski J, Lubiński P. Geometrical  
370 effects in antiproton annihilation on nuclei. *Phys Rev C*  
371 2001;63:027301.

372 [15] Markiel W, Daniel H, von Egidy T, Hartmann FJ, Hofmann P,  
373 Kanert W, et al. Emission of helium ions after antiproton  
374 annihilation in nuclei. *Nuclear Physics A* 1988;485:445–60.

375 [16] Polster D, Hilscher D, Rossner H, von Egidy T, Harmann FJ,  
376 Hoffmann J, et al. Light particle emission induced by stopped  
377 antiprotons in nuclei: energy dissipation and neutron-to-  
378 proton ratio. *Phys Rev C* 1995;51:1167–80.

[17] Holzscheiter Michael H, Bassler Niels, Agazaryan Nzhde, Beyer  
379 Gerd, Blackmore Ewart, DeMarco John J, et al. The biological  
380 effectiveness of antiproton irradiation. *Radiother Oncol*  
381 2006;81:233–42.

[18] Fassò A, Ferrari A, Ranft J, Sala PR. FLUKA: a multi-particle  
382 transport code. CERN-2005-10, INFN/TC\_05/11, SLAC-R-773.  
383

[19] The physics models of FLUKA: status and recent developments,  
384 La Jolla, CA, USA, 2003. (paper MOMT005), eConf C0303241  
385 (2003), arXiv:hep-ph/0306267.

[20] Hansen JW, Olsen KJ, Wille M. The alanine radiation detector  
386 for high and low LET dosimetry. *Radiat Prot Dosimetry*  
387 1987;19:43–7.

[21] Palmans H. Effect of alanine energy response and phantom  
388 material on depth dose measurements in ocular protons  
389 beams. *Technol Cancer Res Treat* 2003;2:579–86.

[22] Niels Bassler, Johnny W. Hansen, Hugo Palmans, Michael H.  
390 Holzscheiter, Sandra Kovacevic, The AD-4/ACE Collaboration.  
391 The antiproton depth dose curve measured with alanine  
392 detectors, Submitted to NIM B. Q3 397

[23] Niels Bassler. Experimental studies relevant for antiproton  
393 cancer therapy. Ph.D. thesis, Aarhus University, 2006. 398

[24] Boag JW, Currant J. Current collection and ionic recombina-  
394 tion in small cylindrical ionization chambers exposed to pulsed  
395 radiation. *Brit J Radiol* 1980;53:471–8. 400

[25] Kanai Tatsuaki, Sudo Michio, Matsufujii Naruhiro, Futami  
396 Yasuyuki. Initial recombination in a parallel-plate ionization  
397 chamber exposed to heavy ions. *Phys Med Biol*  
398 1998;43:3549–58. 401

[26] Gudowska Irena, Sobolevsky Nikolai, Andreo Pedro, Belkič  
399 Dževad, Brahme Anders. Ion beam transport in tissue-like  
400 media using the monte carlo code SHIELD-HIT. *Phys Med Biol*  
401 2004;49:1933–58. 402

[27] Krämer M, Jäkel O, Haberer T, Kraft G, Schardt D, Weber U.  
402 Treatment planning for heavy-ion radiotherapy physical beam  
403 model and dose optimization. *Phys Med Biol* 2000;45:3299–317. 404

[28] Krämer M, Scholz M. Treatment planning for heavy-ion  
404 radiotherapy calculation and optimization of biologically  
405 effective dose. *Phys Med Biol* 2000;45:3319–30. 406

[29] Bassler N, Holzscheiter MH, Jäkel O, Kovacevic S, Knudsen HV,  
406 The AD-4/ACE Collaboration. The antiproton depth-dose  
407 curve in water. Submitted to *Phys Med Biol*. 408

[30] Scholz M. Grundlagen der biologischen Bestrahlungsplanung  
408 für die Schwerionen-Tumorthherapie. Medizinische Fakultät  
409 Heidelberg, Ruprecht-Karls-Universität. Habilitationsschrift.  
410 (In German). 411

[31] Scholz M, Kraft G. Track structure and the calculation of  
411 biological effects of heavy charged particles. *Adv Space Res*  
412 1995;18:5–14. 413

[32] Scholz M, Kellerer AM, Kraft-Weyrather W. Computation of cell  
413 survival in heavy ion beams for therapy. *Radiat Environ Biophys*  
414 1997;36:59–66. 415

Appendix B:  
Physics in Medicine and Biology 2008, in press

## The antiproton depth–dose curve in water

N Bassler<sup>1,2</sup>, M H Holzscheiter<sup>3</sup>, O Jäkel<sup>2</sup>, H V Knudsen<sup>4</sup>, S Kovacevic<sup>5</sup>  
and (the AD-4/ACE Collaboration)<sup>6</sup>

See endnote 1

<sup>1</sup> Department of Experimental Clinical Oncology, Aarhus University Hospital, Aarhus, Denmark

<sup>2</sup> Deutsches Krebsforschungszentrum, Heidelberg, Germany

<sup>3</sup> University of New Mexico, Albuquerque, NM, USA

<sup>4</sup> Department of Physics and Astronomy, University of Aarhus, Aarhus, Denmark

<sup>5</sup> University of Montenegro, Podgorica, Montenegro

E-mail: [n.bassler@dkfz.de](mailto:n.bassler@dkfz.de)

Received 19 September 2007, in final form 2 December 2007

Published DD MMM 2008

Online at [stacks.iop.org/PMB/53/1](http://stacks.iop.org/PMB/53/1)

### Abstract

We have measured the depth–dose curve of 126 MeV antiprotons in a water phantom using ionization chambers. Since the antiproton beam provided by CERN has a pulsed structure and possibly carries a high-LET component from the antiproton annihilation, it is necessary to correct the acquired charge for ion recombination effects. The results are compared with Monte Carlo calculations and were found to be in good agreement. Based on this agreement we calculate the antiproton depth–dose curve for antiprotons and compare it with that for protons and find a doubling of the physical dose in the peak region for antiprotons.

(Some figures in this article are in colour only in the electronic version)

### 1. Introduction

The basic idea of antiproton radiotherapy (Gray and Kalogeropoulos 1984) is to utilize the energy from the antiproton–nucleus annihilation reactions, which occur when the antiprotons come to rest. Antiprotons behave similar to protons at high velocities, but when they slow

<sup>6</sup> M H Holzscheiter 1, N Bassler 2, 3, J Alsner 2, G Beyer 4, J J DeMarco 5, M Doser 6, D Hajdukovic 7, O Hartley 4, K S Iwamoto 5, O Jäkel 3, H V Knudsen 8, S Kovacevic 7, S Pape Møller 9, J Overgaard 2, J B Petersen 2, T D Solberg 10, S Vranjes 11, B G Wouters 12.

1. University of New Mexico, Albuquerque, NM, USA; 2. Department of Medical Physics and Experimental Clinical Oncology, Aarhus University Hospital, Aarhus, Denmark; 3. Deutsches Krebsforschungszentrum, Heidelberg, Germany; 4. Hospital Universitaire de Geneve, Geneva, Switzerland; 5. David Geffen School of Medicine, UCLA, Los Angeles, CA, USA; 6. CERN, Geneva, Switzerland; 7. University of Montenegro, Podgorica, Montenegro; 8. Department of Physics & Astronomy, University of Aarhus, Aarhus, Denmark; 9. ISA, University of Aarhus, Aarhus, Denmark; 10. University of Nebraska Medical Center, Omaha, NE, USA; 11. VINCA Institute for Nuclear Sciences, Belgrade, Serbia; 12. University of Maastricht, Res. Institute Growth and Development, The Netherlands.

down in the target material, they are captured by a nucleus and annihilate on its surface. Hereby twice the rest mass of the proton  $m_p$  is released (1.88 GeV) at the end of the particle trajectory. The probability for photo-emission similar to that known from the positron–electron annihilation is rather small. Instead, on average 4–5  $\pi$ -mesons are created (Inokuti 1989). The photons observed from the antiproton annihilation arise primarily from  $\pi^0$  decay, which has a lifetime in the order of  $10^{-16}$  s. The energy of these photons is between 70 and 300 MeV (Agnew *et al* 1960). For antiproton–nuclei reactions, there is a high probability that one or more  $\pi$ -mesons will strike the nucleus<sup>7</sup>. Those entering the nucleus will start an intra-nuclear cascade, knocking out light nuclei (Markiel *et al* 1988). When antiprotons enter a chemical compound consisting of several materials, the majority of the annihilations will take place on high-Z materials (Ponomarev 1973). For example, in the case of polystyrene only 1% of the antiprotons will annihilate on hydrogen with the remaining 99% annihilating on carbon. Antiprotons annihilating on tissue-like material are expected to produce a particle spectrum featuring pions, neutrons, protons, deuterons, heavier nuclei and photons. A few kaons may also be created (Agnew *et al* 1960, Polster *et al* 1995). Most of the 1.88 GeV released is carried away from the annihilation vertex by the long-ranging particles (high-energy pions, protons, neutrons, and photons), but roughly 30 MeV is deposited locally near the annihilation vertex (Sullivan 1985). Even though this sounds at first sight disappointingly low (Sullivan 1985, Inokuti 1989), it represents a doubling of the peak dose at the end of the antiproton particle track, compared to protons, producing a significant clinical advantage. The loss of the primary beam due to in-flight nuclear reactions is expected to be slightly more than for protons, but still less than that of carbon ions (Bassler *et al* 2005). The antiproton depth–dose curve will therefore look similar to the depth–dose curve of protons, but with additional energy deposited in the Bragg peak from the antiproton annihilation.

Since 2002 the AD-4/ACE Collaboration has been working at CERN, using the antiproton decelerator (AD), on assessing the dosimetric and radiobiological properties of beams of antiprotons in order to estimate the suitability of antiprotons for radiotherapy (Holzscheiter *et al* 2004, 2006, Maggiore *et al* 2004, Bassler *et al* 2006, Bassler 2006). The AD has been designed and constructed for fundamental research on matter–antimatter symmetries and the availability of antiprotons for applied studies is sparse at best. Typically, we are able to obtain one week of beam time each year and have therefore concentrated on collecting few but critical data to benchmark computer models that can then be used to develop treatment planning tools. These in turn will allow us to gain a deeper insight in the potential advantages of antiprotons compared to other modalities and in selecting the most appropriate candidates of tumour indications for antiproton therapy.

Radiotherapy with antiprotons has a potential to deliver a high biological effective dose to the target while at the same time reducing the dose to normal tissue in the entrance region much more than possible with any other radiation modality. It is one of the paradigms of radiotherapy that a decrease of the irradiated volume of normal tissue is in many cases associated with an increased tolerance dose of these tissues (see, e.g., Hopewell and Trott (2000)). There are at least two situations in which antiprotons might be useful for radiotherapy. The first are tumours that cannot be controlled by conventional radiation, because the applied dose is limited by the surrounding normal tissues and where a substantial dose escalation may be beneficial, like e.g. tumours at the base of skull or paraspinal tumours. Another indication may be recurrent tumours. If the initial treatment included any kind of radiotherapy, the normal tissue surrounding the tumour will have already received a significant dose. In order to re-irradiate

<sup>7</sup> For nuclei with  $60 \leq A \leq 200$  the probability is 85–90% according to Cugnon *et al* (2001).



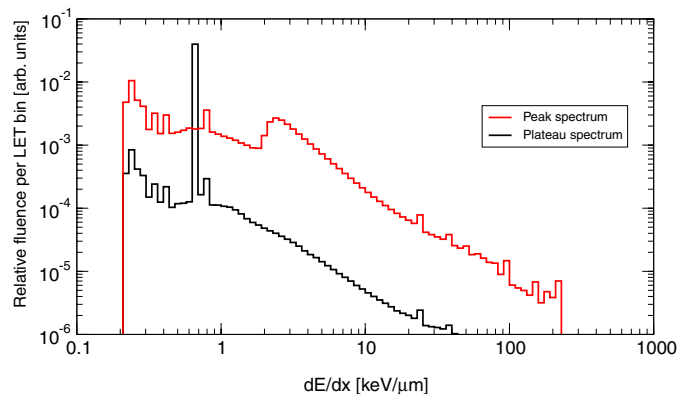


**Figure 1.** FLUKA calculation of charged particle LET spectrum of a 126 MeV antiproton beam. The spectrum was calculated both in the peak region and in the plateau region. Charged particles with  $1 \leq Z \leq 6$  were here taken into account. The sharp line in the plateau region at  $0.6 \text{ keV } \mu\text{m}^{-1}$  originates from the primary antiproton beam.

this tumour one needs to assure that the dose to normal tissue does not exceed accepted tolerance level. This is facilitated by the high peak-to-plateau ratio offered by antiprotons.

Unlike protons, the relative biological effectiveness (RBE) of the antiproton beam varies sharply with depth near the end of range, as the annihilation process yields fragments with a higher linear energy transfer (LET). A calculated LET spectrum is shown in figure 1.

This enhanced LET results in an increased RBE in the peak region relative to the plateau region. The biological effect of an antiproton beam was for the first time measured by Holzscheiter *et al* (2006). However the RBE in the peak could not be measured, since the dosimetry in this region was complicated by both the mixed particle spectrum and the pulsed form of the antiproton beam. Dosimetry with alanine, thermoluminescent devices and radiochromic films were used, but these suffer from a strong, often not well understood, LET dependence of the response. Calorimetric measurements were considered as too cumbersome. Ionization chamber measurements were initially believed to be complicated due to the pulsed structure of the antiproton beam currently available at CERN.

In this paper, we report the first measurement of the dose deposited in water by a pulsed antiproton beam using ionization chambers. The high instantaneous dose rate causes a reduction in the charge collection efficiency due to general recombination effects. Using the ‘Boag’s two voltage method’ as described by Boag and Curren (1980) we can get an estimate of the charge collection efficiency. It should be stressed that our goal is not to perform high precision dosimetry, as there are several sources of errors in the 1% range that may perturb the results which we cannot yet control. Our primary goal is instead to obtain an initial estimate of the RBE for antiprotons that will allow us to define any significant advantages of antiproton radiotherapy over other modalities. For this, uncertainties in dose of a few per cent may be tolerated.

## 2. Experimental methods

The antiproton decelerator (AD) at CERN is set up to provide a  $502 \text{ MeV}/c$  ( $\sim 126 \text{ MeV}$ ) antiproton beam. Every 90 s a spill of roughly  $2\text{--}3 \times 10^7$  antiprotons is ejected within 300 ns. The average number of ejected antiprotons may change depending on the actual state of the

accelerator facility. Using, e.g., arbitrarily selected 20 consecutive spills (corresponding to about 30 min of operation), the average amount of antiprotons per spill was  $2.5 \times 10^7$  with a standard deviation of  $0.1 \times 10^7$ . The number of antiprotons for each spill was recorded for each individual spill using a sensitive current transformer in the extraction beam line from the AD to our target station. While the statistical fluctuations of these measurements are low, particle loss between the transformer and our target may introduce a systematic shift ( $\lesssim 10\%$ ). The momentum spread of the beam was  $\Delta p/p = 5 \times 10^{-4}$ , and the divergence is in the order of 5 mrad. The FWHM of the beam was slightly ellipsoid, being about 1 cm in one axis and 0.9 cm along the other axis. The beam exits the accelerator vacuum via a thin titanium window, traverses several beam monitors (scintillator viewed by CCD camera, radiochromic film) and is collimated to 1 cm diameter before entering our target. The temperature in the AD hall is maintained at 20 °C.

The target phantom is a 220 mm  $\times$  275 mm  $\times$  180 mm water tank built of PMMA material according to IAEA and ICRU standards for proton therapy (IAEA 2000, ICRU 1998). The PMMA walls are all 10 mm thick, except for the entrance window, which is 3 mm thick and had a diameter of 70 mm. We use two custom-made plane-parallel ionization chambers of the advanced Roos type from PTW Freiburg with graphite electrodes<sup>8</sup>. These are similar to the standard Roos chamber M34001, but with an increased diameter of 39.6 mm and a collecting volume of 2.479 cm<sup>3</sup>. The electrode spacing is 2.013 mm. The ionization chambers are cross calibrated in absorbed dose to water using <sup>60</sup>Co  $\gamma$ -rays as reference radiation quality at +400 V towards a reference ionization chamber using the in-house gammatron at the German Cancer Research Center (DKFZ) in Heidelberg (Kartal 2007). The calibration is carried out with a 10 cm  $\times$  10 cm field in a water phantom at 20 °C temperature and air pressure of 1013 hPa. The source–chamber distance was 80 cm and the measurement depth in water was 5 g cm<sup>-2</sup> for the effective point. The reference chamber is a PTW Roos ionization chamber M34001-0045 and is calibrated at PTW, which is a Secondary Standard Dosimeter Laboratory (SSDL). The  $N_{D_0}$  is found to be  $1.32 \times 10^7$  Gy C<sup>-1</sup> for both ionization chambers with an uncertainty of  $\pm 4\%$ .

The measurement in the antiproton beam was performed using a pencil beam which had a diameter that was much smaller than the active area of the chamber. The dose obtained under such conditions is an integral dose over the area of the chamber at the specific depth rather than a central axis depth dose which is measured in a broad beam. Measuring such an integral dose is common for facilities using, e.g., a scanned pencil beam, like at the Paul-Scherrer institute or at GSI for carbon ions.

At the antiproton beam line at CERN, one ionization chamber is attached in front of the entrance window to the water phantom. This chamber is used for normalization of the pulse to pulse fluctuations of the antiproton beam. The second chamber is attached to a calliper which provides submillimetre precision readings of the ionization chamber position. The collected charge is read out with a UNIDOS electrometer from PTW Freiburg.

At each calliper position, data from each of several spills of antiprotons are recorded. Typically, we see around 175 pC per spill in the entry chamber and 0.2–1.4 nC in the second ionization chamber depending on the position in the water phantom. The fixed ionization chamber at the entrance window is kept at +400 V at all times. With the ionization chamber mounted in the water phantom we usually record 4–8 spills at +400 V and 4 spills at +300 V. The electrometer is read out and reset after each spill. The dark current contribution was insignificant.

<sup>8</sup> TM34073-1, 08-0001 and -0002.

From the measured charge  $q_1$  and  $q_2$  recorded at  $V_1 = 400$  V and  $V_2 = 300$  V, respectively, it is possible to apply Boag's theorem Boag and Currant (1980). This is done by solving

$$0 = \frac{q_1}{q_2} \cdot \frac{V_2}{V_1} - \frac{\ln(1 + u_1)}{\ln(1 + u_1 V_1 / V_2)}. \quad (1)$$

Equation (1) is derived from equation (9) in (Boag and Currant 1980).  $u$  is related to the collection efficiency  $f$  in such a way that

$$f = \frac{1}{u} \ln(1 + u). \quad (2)$$

In practice, a plug-in was written<sup>9</sup> for the 'Gnumeric' spreadsheet program<sup>10</sup>, which extended the software with additional functions for calculating  $u$  and  $f$ . As an input parameter the measured charges at two voltages are needed. The functionality of the algorithms was checked by comparing the results with another independently developed program using the root-finding function provided by the Gnu Scientific Library (Galassi *et al* 2007).

Alternatively, Boag *et al* also suggest three different algorithms in Boag *et al* (1996) which enhance equation (2) with a free-electron collection effect on the recombination correction. These three algorithms are also supported in the plug-in mentioned before. In these algorithms, the free-electron fraction  $p$  is needed as an additional parameter. In this paper,  $f'$  will be the free-electron-corrected charge collection efficiency based upon equation 7 in Boag *et al* (1996):

$$f'(u) = f(u) \cdot \frac{e^{pu} - 1}{pu}. \quad (3)$$

At some calliper positions, we only measure charge at one voltage setting (400 V). Here, the charge collection efficiency is interpolated from neighbouring positions. Beyond the annihilation peak the acquired charge is small and equation (1) has no solution due to statistical fluctuations, and instead the collection efficiency is extrapolated. Similarly for the ionization chamber at the fixed entry position, the charge collection efficiency is merely estimated by extrapolation.

Linearity checks validating Boag's two voltage method are made at two calliper positions, covering the peak and the plateau region. Here the entire voltage range from the UNIDOS electrometer is applied in 50 V steps, and the  $q^{-1}$  versus  $V^{-1}$  plots are investigated for linearity.

The Boag-corrected collected charge  $M_{Q,B}$  of the antiproton beam quality  $Q$  can be found by

$$M_{Q,B} = q/f. \quad (4)$$

The absolute dose  $D_Q$  is then

$$D_Q = M_{Q,B} N_{Q_0} k_{Q,Q_0} \quad (5)$$

where  $N_{Q_0}$  is the <sup>60</sup>Co calibration factor, as mentioned earlier.  $k_{Q,Q_0}$  is a beam quality correction factor, which here is set to unity. The  $k_{Q,Q_0}$  factor for the advanced Roos chamber should be nearly identical to the corresponding factor for the standard Roos chamber, the only possible difference being the chamber specific correction factors  $p_Q$  appearing in the calculation of  $k_{Q,Q_0}$  (according to equation (3.4) of IAEA (2000)). This  $p_Q$  factor is, however, taken to be unity for all chambers in a proton beam in IAEA (2000) and for photons the only effect of an increased diameter could influence the perturbation effect of the wall,  $p_{\text{wall}}$ , which is given as 1.001 for the Roos chamber. Given the large guard ring of the Roos chamber this factor should be dominated by the entrance and exit window of the chamber. Any expected

<sup>9</sup> The plug-in is available at <http://www.phys.au.dk/~bassler/work.shtml?Boag>.

<sup>10</sup> <http://www.gnome.org/projects/gnumeric/>.

difference for our chamber should not exceed the 1% level, an accuracy that is clearly beyond the level of accuracy we are aiming for in our experiment. A difference in  $k_{Q,Q_0}$  for protons and antiprotons may arise due to the different spectra of secondary particles. Even for carbon ions, where secondary particles may play a similarly important role as for antiprotons,  $k_{Q,Q_0}$  is still assumed to be of the same range as for protons, namely 1.003. Taking  $k_{Q,Q_0}$  as unity for antiprotons is thus not expected to introduce an uncertainty of more than 1–2%.

The relative measurements plotted in figures 5 and 6 are the ratio between the Boag-corrected charge measured in the ionization chamber mounted on the calliper  $M_{Q,B,\text{var}}(d)$  at a given depth  $d$  and the charge measured in the entry ionization chamber  $M_{Q,B,\text{entry}}$  corresponding to a water-equivalent (WE) depth of  $d = 0$  cm:

$$\frac{M_{Q,B,\text{var}}(d)}{M_{Q,B,\text{entry}}} = \frac{q_{\text{var}}(d)}{q_{\text{entry}}} \cdot \frac{f_{\text{entry}}}{f_{\text{var}}(d)}. \quad (6)$$

As mentioned earlier, the average ratio was acquired from multiple spills. The absolute measurements presented in the third column in table 1 is the dose per antiproton, calculated using equation (5) and the number of antiprotons derived from the beam current monitor. The dose per antiproton presented here is averaged over multiple spills as well, and the standard deviation of the measurement is mentioned in the table as well.

### 3. Monte Carlo calculations

For comparison, calculations using both FLUKA v. 2006.3 (Fassò *et al* 2005, eConf C0303241:MOMT005 2003) and SHIELD-HIT v2.2 (Gudowska *et al* 2004) are applied. The geometry applied in FLUKA and SHIELD-HIT consists simply of a 502 MeV/c antiproton beam hitting a  $20 \times 20 \times 20$  cm<sup>3</sup> water tank. The Gaussian-shaped beam width was set to have a FWHM of 1.0 cm and 0.9 cm along the  $x$ - and  $y$ -axes. For statistical precision we used 150 000 and 100 000 primary particles, respectively, in the calculations using FLUKA and SHIELD-HIT.

The scoring region is a stack of discs placed along the beam axis. Each disc has a diameter of 39.6 mm matching the effective diameter of the ionization chamber. Since the FWHM of the beam width is only in the order of 1 cm, practically all antiprotons are contained in the active scoring region, even in the Bragg peak. This is illustrated in figure 2 which shows the lateral dose profile for the simulated beam in the plateau and the peak regions. The active scoring region also includes most low energy fragments generated in the annihilation events.

The resolution along the beam axis was in 1 mm steps for the SHIELD-HIT simulation and 0.25 mm for the FLUKA simulation. For all FLUKA calculations a beam momentum spread of  $\Delta p/p = 5 \times 10^{-4}$  was used as well as a beam divergence of 5 mrad, corresponding to the characteristics of the CERN beam. In FLUKA, the default transport settings and cut-off energies from the ‘HADROTHE’ card are always used.

For comparison with protons (shown later in figure 7), the FLUKA calculation was repeated using a  $5 \text{ cm} \times 5 \text{ cm}$  square field of antiprotons, while maintaining beam energy, momentum spread and divergence. The target was a  $20 \times 20 \times 100$  cm<sup>3</sup> water tank placed along the beam axis. The average dose is again scored along the beam axis using flat discs, but with a radius of 0.5 cm and a thickness of 0.25 mm. Here, 400 000 particles are simulated.

Finally, the LET spectrum shown in figure 1 was obtained using 400 000 particles in a water phantom. Again, the primary beam was a  $5 \text{ cm} \times 5 \text{ cm}$  square field of antiprotons with unchanged beam energy, momentum spread and divergence. The track-length fluence was scored for pions and kaons ( $\pi^+$ ,  $\pi^-$ ,  $\pi^0$ ,  $K^+$ ,  $K^-$ ,  $K^0$ ), for protons and antiprotons, as well as all other nuclei with  $1 \leq Z \leq 6$ . The scoring region was one  $2 \times 2 \times 1$  cm<sup>3</sup> box placed at

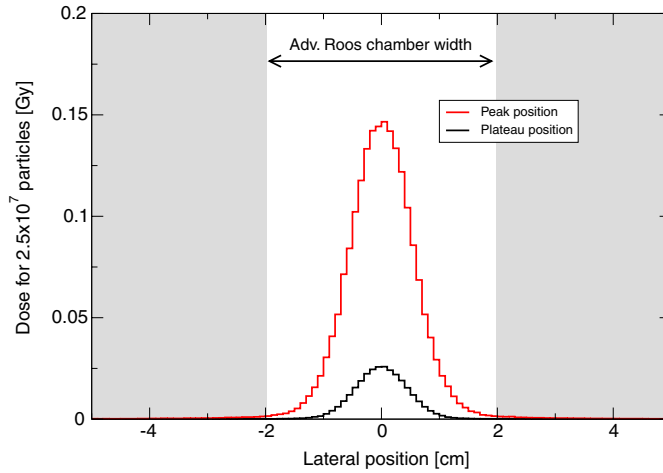


**Figure 2.** FLUKA calculation of the lateral dose distribution at 1.1 cm WE depth and 11.6 cm depth for the CERN beam. The entire beam is confined within the diameter of the ionization chamber.

the entrance to the water phantom in the centre of the beam with the short sides parallel to the beam axis. A similar scoring volume is also positioned around the centre of the annihilation peak at a depth of 11–12 cm.

Initial attempts to use Geant4 (Allison *et al* 2006, Agostinelli *et al* 2003) failed, as at that time the behaviour of very low energy antiprotons had not yet been fully incorporated. Meanwhile much progress in this area has been made (Kossov 2005) and future studies may include Geant4 simulations.

#### 4. Results

The  $1/q$  versus  $1/V$  plot in the plateau and at the peak of the depth–dose curve is shown in figure 3. The data were normalized to  $1/q$  acquired at 400 V. The choice of 400 and 300 V for the ionization chamber may not be ideal, as it is often suggested that  $V_1 > 2V_2$ . However, these voltage setting are within the region of linearity for the entire depth–dose curve, thereby maintaining a consistent read-out procedure.

The calculated charge collection efficiency,  $f$ , which was applied to the measured charge, is shown in figure 4 as a function of WE depth. Using the charge collection efficiency data, we can compare the measured depth–dose curve in water with SHIELD-HIT and FLUKA simulations, which is shown in figures 5 and 6, respectively. Since the measurements were recorded with an arbitrary  $x$ -scale, the measurements were shifted along the  $x$ -axis in order to match the peak of the Monte Carlo calculations. Both the Monte Carlo calculations and the measurements are normalized to unity at 88 mm WE depth in order to better show the deviations in the form of the depth–dose curve. Using this normalization, the SHIELD-HIT calculations show an overestimation of more than 20% in the peak region, whereas FLUKA matches the measured depth–dose curve very well ( $\lesssim 1\%$ ). In the plateau region at 38.5 mm WE depth SHIELD-HIT underestimates the relative dose with 16%. FLUKA overestimates the dose here with less than 2%.

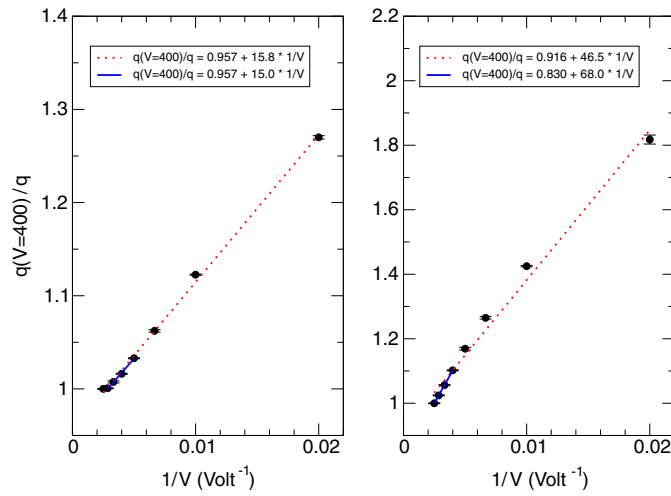


**Figure 3.**  $1/q$  versus  $1/V$  plots. Left figure shows data acquired in the plateau region, the right figure is acquired in the peak region. Results are normalized at  $1/q$  ( $V = 400$ ).

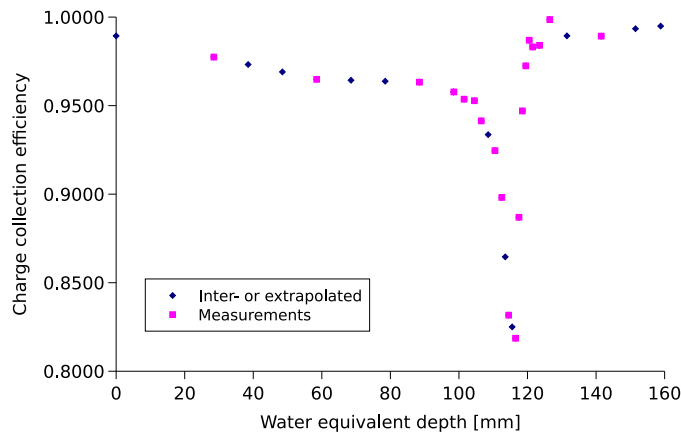


**Figure 4.** Calculated charge collection efficiency.

In terms of absolute values, our measurements indicate higher doses than calculated with SHIELD-HIT or FLUKA. With the entry ionization chamber we measure on average  $101 \pm 4$  pGy (pGy) deposited dose per antiproton. As an estimate, we extrapolate the charge collection efficiency from the first data points of the second ionization chamber. At the second ionization chamber we see  $116 \pm 2$  pGy of deposited dose per antiproton in a WE depth of 28 mm and  $166 \pm 3$  pGy at a WE depth of 88 mm. In table 1, we compare these values to those calculated by SHIELD-HIT and FLUKA. The errors stated here are  $1\sigma$  standard deviations.

The free-electron effect was calculated at a point in the plateau (at 28 mm WE depth) and the peak region (at 116 mm WE depth) assuming  $p = 0.1$ . The results are presented in table 2.

All data and data analysis are made available on the world wide web (Bassler *et al* 2007).

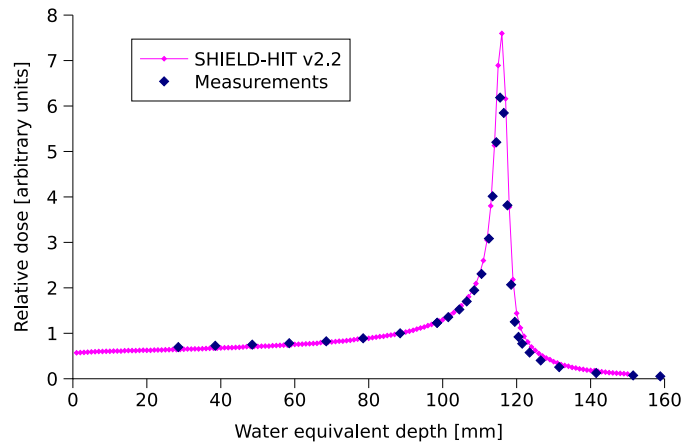


**Figure 5.** 126 MeV antiprotons hitting a water target. SHIELD-HIT v.2.2 Monte Carlo calculations compared with ionization chamber measurements.

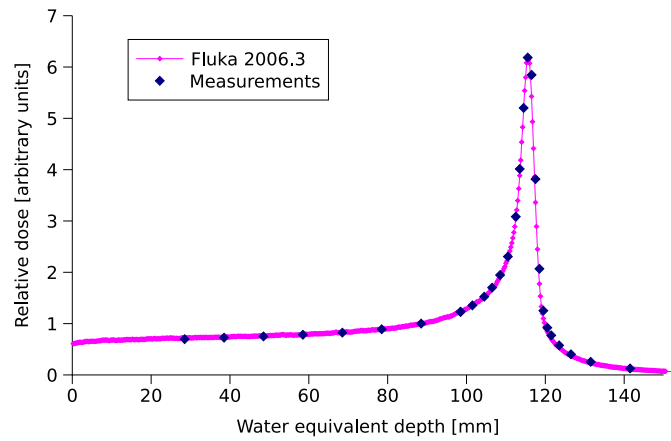


**Figure 6.** 126 MeV antiprotons hitting a water target. FLUKA 2006.3 Monte Carlo calculations compared with ionization chamber measurements.

**Table 1.** Absolute comparison of deposited dose per antiproton.

	SHIELD-HIT (pGy)	FLUKA (pGy)	Measurements (pGy)
Entry chamber at 0 mm	86.7	96.7	101 ± 4
Chamber at 27.5 mm	94.5	109	116 ± 2
Chamber at 87.5 mm	147	152	166 ± 3

## 5. Discussion

We found excellent agreement between ionization chamber measurements and FLUKA simulations for relative dose and reasonable agreement in the plateau regions for absolute dose (error < 4–9%). The origin of the systematic deviation between experiment and models is not clear, but may possibly be attributed to several sources: first, the advanced Roos chamber

**Table 2.** Collection efficiency without ( $f$ ) and with ( $f'$ ) free-electron correction;  $p = 0.1$ .

	$u$	$f$	$f'$
Chamber at plateau (27.5 mm)	0.0466	0.9774	0.9797
Chamber at peak (115.5 mm)	0.4736	0.8186	0.8383

was cross calibrated towards another ionization chamber which has an uncertainty of  $\pm 4\%$  (Kartal 2007). Second, the calibration of the antiproton beam current monitor (which provides the amount of antiprotons) is accurate to only  $\pm 1\%$  and may additionally have a systematic deviation of up to 10%. The difference in results from SHIELD-HIT and FLUKA is most likely related to different in-flight annihilation cross sections used by the two code packages. The in-flight annihilation cross sections of antiprotons and in-flight losses of other ions are discussed in more detail in Bassler *et al* (2005).

From the presented data it is difficult to decide which of the two code packages gives a more accurate value for the absolute antiproton dose. But based on the better agreement of the relative dose versus depth and on the fact that FLUKA simulations of protons were benchmarked by Biaggi *et al* (1999) and found in very good agreement with measurements, we tend to favour the FLUKA code package.

Finally, there is an uncertainty coming from the application of Boag's theory to the antiproton beam. The correction used is strictly valid only if the linearity of the  $1/q$  versus  $1/V$  plot is maintained. In figure 3, the plateau position plot reveals a deviation from linearity at a chamber voltage of 400 V. But when using points from 350 V and below, this only changed the charge collection efficiency by roughly 1.5%. The data in figures 5 and 6 are exclusively based on charge collected at 400 V and 300 V.

For pulsed beams both initial and general recombination show a linear  $1/q$  versus  $1/V$  dependence (Palmans *et al* 2006). In principle, it is possible to distinguish the contributions from both recombination effects. By varying the pulse length, only the general recombination is affected, as initial recombination is independent of the incident dose rate (Park *et al* 2006). Since it is not possible to significantly change the pulse length at the CERN beam line, one could instead change the angle of the ionization chamber relative to the beam axis. This was done by Kanai *et al* (1998) for a heavy ion beam, which also investigated the LET dependence of initial recombination. It could be interesting to apply similar methods to the antiproton beam in a future experiment and perhaps derive an estimate of the mean LET of the particle spectrum.

The result from Boag's free-electron-correction term in table 2 indicates only small changes to the result. The change of the charge collection efficiency when applying  $f'$  instead of  $f$  is less than 1% in the plateau region and 2% in the peak region. The other two models in Boag *et al* (1996) gave similar results within  $\sim 1\%$ . The estimate of  $p = 0.1$  was derived from figure 3 in that reference. Here,  $p$  is plotted as a function of  $V$  for a plane-parallel ionization chamber with an electrode distance of 6.1 mm. Assuming equal field strength in the ionization chamber we read out  $p$  for a corresponding electrode distance of 2 mm. As a test, we tried to minimize the sum-of-squares deviation between measurement and FLUKA calculation and use  $p$  as a free parameter. A best fit was then achieved at  $p = 0.062$ , but this is regarded as being highly speculative.

At last, one may discuss whether the Bragg–Gray conditions are fulfilled for an antiproton beam. Antiprotons annihilating on the air in the ionization chamber may lead to the generation of new particles, leading to a violation of the charged particle equilibrium requirement.



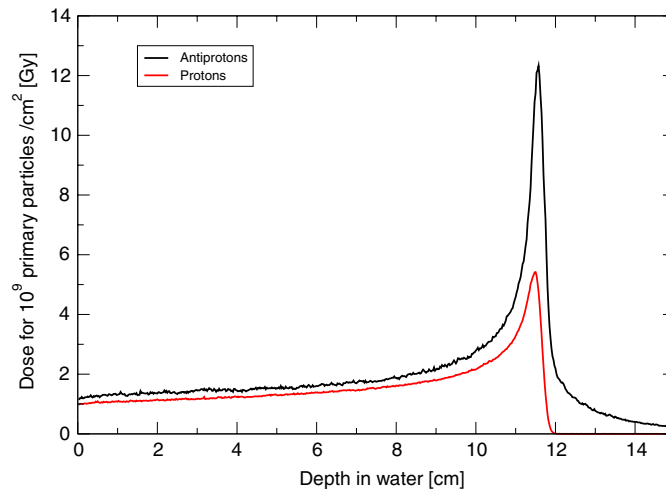


**Figure 7.** Comparison of the central axis depth–dose curves in water from a pristine antiproton beam with a similar proton beam. The depth–dose curves were calculated with FLUKA. The energy of the antiprotons was 126 MeV, and the field size was 5 cm  $\times$  5 cm. The momentum spread was assumed to be  $\Delta p/p = 5 \times 10^{-4}$  and the beam divergence was set at 5 mrad. The dose was scored along a cylindrical region with a diameter of 1 cm in 0.25 mm steps.

Those particles may have different energy spectrum and composition. But as air mostly consists of light elements such as oxygen and nitrogen which are comparable to carbon<sup>11</sup> and the water environment, we do not expect significant deviations here. Despite the various uncertainties mentioned above, the overall agreement between FLUKA and our experimental data provides us with a reasonable level of confidence that we can determine dose–depth curves for antiprotons with sufficient accuracy to obtain RBE values versus depth for an antiproton beam using the measured survival values obtained in previous (Holscheiter *et al* 2006) and future experiments conducted at CERN.

If the dosimetric evaluation is confirmed further, this will emphasize the potential of antiprotons in radiotherapy compared to protons, as presented in figure 7. Here, we used a broad beam (5 cm  $\times$  5 cm) in order to more closely match a clinical situation. In principle, this beam could be produced passively or actively to cover the target area. Scoring the central dose region, several features can be observed. In the entry region, a slight elevation of the dose level is seen as compared to protons, arising from antiprotons annihilating in-flight. The peak region itself is augmented by a factor of more than two as compared with the proton Bragg peak, at iso-fluence. When peak normalizing the depth–dose curves shown here, the dose from antiprotons at a depth of 6 cm will only be half that of the dose from protons, illustrating the significant reduction in normal tissue dose for an identical physical dose to the tumour. Combining the results obtained here and the RBE estimate in (Holscheiter *et al* 2006) of around 2 (for a slightly spread-out annihilation peak), this imposes an even further decrease of the biologically effective dose in the entrance region as compared to a proton beam with identical biological effect in the target region.

<sup>11</sup> Ionization chamber electrodes consist of carbon, and the plastic housing is expected to consist of a carbon-rich compound too.

The comparison of proton and antiproton depth–doses at the same range shows the immense potential of antiprotons to reduce the dose to normal tissue in the entrance region of the particles, even without taking any increase in biological efficiency into account.

It should of course be mentioned that the dose beyond the Bragg peak is non-negligible in the case of antiprotons, which is due to the annihilation products. This dose contribution, however, is not a major concern for most clinical applications and both smaller in value and of shorter range than the dose in the fragment tail of, e.g., carbon ions. Thus, the improvement of the depth–dose characteristic of antiprotons as compared to protons seems to be undoubted. The remaining open question to be answered is the lateral dose distribution from antiprotons, especially close to the annihilation region. If the dose due to secondary particles is spread out significantly more in the lateral direction as compared to protons, this may be a serious drawback for the clinical use of antiprotons. Since the annihilation event happens at rest and is therefore isotropic in its effect we can already deduce some information from the distal edge of the Bragg peak. From our earlier measurements (Holzscheiter *et al* 2006) we expect the penumbra of antiproton beams to be only slightly larger than for protons. In addition, the effect of the diffuse and apparently weak dose from pions, gammas and neutrons on tissue far from the target area needs to be considered.

We are currently investigating this topic with model calculations along with experiments attempting to assess the peripheral dose, and this work will be the subject of a future publication which is in preparation.

## 6. Conclusion

Simulations with FLUKA 2006.3 are in excellent agreement with our relative measurements. In terms of absolute dose, our measurements are 6–9% higher than the FLUKA calculations, but this may be attributed to uncertainties in the saturation correction, the Monte Carlo simulation, the calibration of the ion chambers or a systematic shift in the number of antiprotons entering the target.

SHIELD-HIT v.2.2 overestimated the peak–plateau ratio, which is most likely related to the annihilation cross sections used by this code. Using ion chamber dosimetry, for the first time an absolute value of the absorbed dose in a beam of antiprotons could be determined. This enables a quantitative evaluation of the relative biological effectiveness of antiprotons and proves the superiority of the depth–dose distribution of antiprotons as compared to protons.

## Acknowledgments

NB thanks the Danish Cancer Society for supporting this project with a grant. We thank Frank Fabian for assisting with the experiments and DKFZ for providing the ionization chambers and electrometers. HK thanks the ICE Center under the Danish Natural Science Research Council for support of this project. We gratefully acknowledge the AD operations team for their ongoing support and interest and for modifying the standard operating cycle of the AD machine to provide us with a higher energy antiproton beam as normally available.

## References

- Agnew L E Jr, Elioff T, Fowler W B, Lander R L, Powell W M, Segrè E, Steiner H M, White H S, Wiegand C and Ypsilantis T 1960 Antiproton interactions in hydrogen and carbon below 200 MeV *Phys. Rev.* **137**1–91
- Agostinelli S *et al* 2003 Geant4—a simulation toolkit *Nucl. Instrum. Methods A* **506** 250–303
- Allison J *et al* 2006 Geant4 developments and applications *IEEE Trans. Nucl. Sci.* **53** 270–8

- Bassler N 2006 Experimental studies relevant for antiproton cancer therapy *PhD Thesis* Aarhus University
- Bassler N, Holzscheiter M and Knudsen H and the AD4/ACE Collaboration 2005 Cancer therapy with antiprotons *Low Energy Antiproton Physics-LEAP'05 (AIP Conference Proceedings vol CP796)* ed D Grzonka, R Czyżykiewicz, W Oelert, T Rożek and P Winter (New York: AIP) pp 423–30
- Bassler N, Knudsen H, Møller S P, Petersen J B, Rahbek D and Uggerhøj U I and the AD4/ACE Collaboration 2006 Bubble detector measurements of a mixed radiation field from antiproton annihilation *Nucl. Instrum. Methods B* **251** 269–73
- Bassler N *et al* 2007 *PBar Data* <http://www.phys.au.dk/bassler/pbar/>
- Biaggi M, Ballarini F, Burkard W, Egger E, Ferrari A and Ottolenghi A 1999 Physical and biophysical characteristics of a fully modulated 72 {MeV} therapeutic proton beam: model predictions and experimental data *Nucl. Instrum. Methods B* **89**–100
- Boag J W and Curren J 1980 Current collection and ionic recombination in small cylindrical ionization chambers exposed to pulsed radiation *Br. J. Radiol.* **53** 471–8
- Boag J W, Hochhäuser E and Balk O A 1996 The effect of free-electron collection on the recombination correction to ionization measurements of pulsed radiation *Phys. Med. Biol.* **41** 885–97
- Cugnon J, Wycech S, Jastrzębski J and Lubiński P 2001 Geometrical effects in antiproton annihilation on nuclei *Phys. Rev. C* **63** 027301
- eConf C0303241:MOMT005 2003 The physics models of FLUKA: status and recent developments *eConf C0303241: Paper MOMT005 (La Jolla, CA, USA, 24–28 March 2003 (Preprint hep-ph/0306267))* **See endnote 2**
- Fassò A, Ferrari A, Ranft J and Sala P R 2005 FLUKA: a multi-particle transport code *CERN-2005-10, INFN/TC\_05/11, SLAC-R-773*
- Galassi M *et al* 2007 GSL—Gnu Scientific Library <http://www.gnu.org/software/gsl/> **See endnote 3**
- Gray L and Kalogeropoulos T E 1984 Possible biomedical applications of antiproton beams: focused radiation transfer *Radiat. Res.* **246**–52
- Gudowska I, Sobolevsky N, Andreo P, Belki D and Brahme A 2004 Ion beam transport in tissue-like media using the Monte Carlo code SHIELD-HIT *Phys. Med. Biol.* **49** 1933–58
- Holzscheiter M H *et al* 2004 Biological effectiveness of antiproton annihilation *Nucl. Instrum. Methods B* **221** 210–4
- Holzscheiter M H *et al* 2006 The biological effectiveness of antiproton irradiation *Radiother. Oncol.* **81** 233–42
- Hopewell J W and Trott K-R 2000 Volume effects in radiobiology as applied to radiotherapy *Radiother. Oncol.* **56** 283–8
- IAEA (International Atomic Energy Agency) 2000 Absorbed dose determination in external beam radiotherapy: an international code of practice for dosimetry based on standards of absorbed dose to water *Technical Report 398* (Vienna: IAEA)
- ICRU (International Commission on Radiation Units and Measurements) 1998 Clinical proton dosimetry: Part I. Beam production, beam delivery and measurement of absorbed dose *Technical Report 59* (Bethesda, MD: ICRU)
- Inokuti M 1989 Interactions of antiprotons with atoms and molecules *Nucl. Tracks Radiat. Meas.* **16** 115–23
- Kanai T, Sudo M, Matsufujii N and Futami Y 1998 Initial recombination in a parallel-plate ionization chamber exposed to heavy ions *Phys. Med. Biol.* **43** 3549–58
- Kartal Ö M 2007 Cross-calibration of ionization chambers for heavy ion beams *Bachelor's Thesis* Institut für Medizinische Physik und Strahlenschutz, FH Giessen, Germany
- Kossov M 2005 Simulation of antiproton–nuclear annihilation at rest *IEEE Trans. Nucl. Sci.* **52** 2832–5
- Maggiore C *et al* 2004 Biological effectiveness of antiproton annihilation *Nucl. Instrum. Methods B* **214** 181–5
- Markiel W *et al* 1988 Emission of helium ions after antiproton annihilation in nuclei *Nucl. Phys. A* **485** 445–60
- Palmans H, Thomas R and Kacperek A 2006 Ion recombination correction in the Clatterbridge Centre of Oncology clinical proton beam *Phys. Med. Biol.* **51** 903–17
- Park S H, Kim Y K, Kim H S, Kang S M and Ha J H 2006 Characteristics of the saturation curve of the ionization chambers in overlapping pulsed beams *Nucl. Instrum. Methods A* **566** 706–12
- Polster D *et al* 1995 Light particle emission induced by stopped antiprotons in nuclei: energy dissipation and neutron-to-proton ratio *Phys. Rev. C* **51** 1167–80
- Ponomarev L I 1973 Molecular structure effects on atomic and nuclear capture of mesons *Annu. Rev. Nucl. Sci.* **395**–430
- Sullivan A H 1985 A measurement of the local energy deposition by antiprotons coming to rest in tissue-like material *Phys. Med. Biol.* **30** 1297–303

## Endnotes

- (1) Author: Please check whether the footnote to the collaboration is OK as set.
- (2) Author: Please provide the names of the authors in reference eConf C0303241:MOMT005 (2003).
- (3) Author: Please check whether the year in references Galassi *et al* (2007) and Bassler *et al* (2007) is OK as set.
- (4) Author: Please be aware that the colour figures in this article will only appear in colour in the Web version. If you require colour in the printed journal and have not previously arranged it, please contact the Production Editor now.

---

## Reference linking to the original articles

References with a volume and page number in blue have a clickable link to the original article created from data deposited by its publisher at CrossRef. Any anomalously unlinked references should be checked for accuracy. Pale purple is used for links to e-prints at arXiv.

# 7 The Antiproton Depth Dose Curve 8 Measured with Alanine Detectors 9

10  
11  
12  
13  
14 Niels Bassler<sup>a,b</sup> Johnny W. Hansen<sup>c</sup> Hugo Palmans<sup>d</sup>  
15 Michael H. Holzscheiter<sup>e</sup> Sandra Kovacevic<sup>f</sup>  
16 and the AD-4/ACE Collaboration<sup>\*</sup>  
17  
18

19 <sup>a</sup>*Department of Experimental Clinical Oncology, Aarhus University Hospital,*  
20 *Aarhus, Denmark*

21  
22 <sup>b</sup>*Deutsches Krebsforschungszentrum, Heidelberg, Germany*

23 <sup>c</sup>*Emeritus, formerly Vejle Hospital, Vejle, Denmark.*

24  
25 <sup>d</sup>*National Physical Laboratory, Teddington, Middlesex, UK*

26  
27 <sup>e</sup>*University of New Mexico, Albuquerque, NM, USA*

28  
29 <sup>f</sup>*University of Montenegro, Podgorica, Montenegro*  
30  
31  
32

---

## 33 Abstract

34  
35  
36 In this paper we report on the measurement of the antiproton depth dose curve,  
37 with alanine detectors. The results are compared with simulations using the par-  
38 ticle energy spectrum calculated by FLUKA, and using the track structure model  
39 of Hansen and Olsen for conversion of calculated dose into response. A good agree-  
40 ment is observed between the measured and calculated relative effectiveness al-  
41 though an underestimation of the measured values beyond the Bragg-peak remains  
42 unexplained. The model prediction of response of alanine towards heavy charged  
43 particles encourages future use of the alanine detectors for dosimetry of mixed ra-  
44 diation fields.  
45  
46  
47

48 *Key words:* alanine, antiproton annihilation, mixed radiation field dosimetry

49 *PACS:* 25.43.+t, 87.53.-j, 87.53.Qc, 87.53.Pb, 87.53.Wz, 87.66.Pm  
50  
51  
52  
53  
54

---

55 <sup>\*</sup> Michael H. Holzscheiter<sup>1</sup>, Niels Bassler<sup>2,3</sup>, Jan Alsner<sup>2</sup>, Gerd Beyer<sup>4</sup>, John J. DeMarco<sup>5</sup>, Michael Doser<sup>6</sup>, Dragan Haj-  
56 dukovic<sup>7</sup>, Oliver Hartley<sup>4</sup>, Keisuke S. Iwamoto<sup>5</sup>, Oliver Jäkel<sup>3</sup>, Helge V. Knudsen<sup>8</sup>, Sandra Kovacevic<sup>7</sup>, Søren Pape Møller<sup>9</sup>,  
57 Jens Overgaard<sup>2</sup>, Jørgen B. Petersen<sup>2</sup>, Osman Ratib<sup>4</sup>, Timothy D. Solberg<sup>10</sup>, Sanja Vranjes<sup>11</sup>, Bradley G. Wouters<sup>12</sup>. 1 Uni-  
58 versity of New Mexico, Albuquerque, NM, USA; 2 Dept. of Medical Physics and Experimental Clinical Oncology, Aarhus  
59 University Hospital, Aarhus, Denmark; 3 Deutsches Krebsforschungszentrum, Heidelberg, Germany; 4 Hospital Universi-  
60 taire de Geneve, Geneva, Switzerland; 5 David Geffen School of Medicine, UCLA, Los Angeles, CA, USA; 6 CERN, Geneva,  
61 Switzerland; 7 University of Montenegro, Podgorica, Montenegro; 8 Dept. of Physics & Astronomy, University of Aarhus,  
62 Aarhus, Denmark; 9 ISA, University of Aarhus, Aarhus, Denmark; 10 University of Nebraska Medical Center, Omaha, NE,  
63 USA; 11 VINCA Institute for Nuclear Sciences, Belgrade, Serbia; 12 University of Maastricht, Res. Institute Growth and  
64 Development, The Netherlands.  
65

1  
2  
3  
4 **1 Introduction**  
5  
6  
7

8 In radiotherapy of deep seated tumours it is advantageous to be able to deliver  
9 the dose from ionizing radiation to the tumour while at the same time sparing  
10 the surrounding normal tissue to maximum possible extend. The depth dose  
11 profile of a proton beam is far superior to the depth dose beam of photons  
12 in such cases, as the deposited energy peaks at the end of the range of the  
13 primary charged particle track.  
14  
15

16 In 1984 Gray and Kalogeropoulos suggested radiotherapy with antiprotons [1].  
17 One of the anticipated advantages of antiprotons compared to protons, is the  
18 additional energy deposited at the Bragg-peak from the antiproton annihila-  
19 tion. Sullivan suggested in [2] that the additional local energy deposited by the  
20 annihilation products may roughly be about 30 MeV over the last  $0.5 \text{ g cm}^{-2}$   
21 of its trajectory. Even though this value sounds low compared with the total  
22 of 1.88 GeV released by the annihilation, this still results in a substantial aug-  
23 mentation of the peak dose at the end of the particle track. Roughly, a proton  
24 has about 20 MeV left of kinetic energy before the onset of the Bragg-peak  
25 (corresponding to a residual range of  $0.5 \text{ g cm}^{-2}$ ) and the additional 30 MeV  
26 would therefore more than double the energy deposited in the peak region.  
27 In this paper we try to characterize the antiproton annihilation peak, using  
28 alanine detectors.  
29  
30  
31  
32  
33

34 To interpret a measured response of a biological system exposed to a beam  
35 of charged particles in terms of dose deposition, a prediction of the Relative  
36 Biological Effectiveness (RBE) for the particular beam of particles is necessary.  
37 Similarly, for a radiation detector the relative effectiveness (RE) is relating the  
38 observed detector response with dose deposition. The observed response of a  
39 detector is here expressed in terms of the dose  $R$ , which is the dose as read  
40 from the  $^{60}\text{Co}$   $\gamma$ -ray response curve. This term will exclusively be used here  
41 to express response. For the dose  $D_{\text{ion}}$  deposited by ions and the secondary  
42 particles produced along the primary beam path, we have  
43  
44  
45

$$46 \quad R_{\text{ion}} = \text{RE} \cdot D_{\text{ion}} \quad (1)$$

47  
48  
49

50 Thus,  $R_{\text{ion}}$  is the response of a detector exposed to ion beams, expressed in  
51 terms of the dose by  $\gamma$ -rays necessary to produce an equal response. Here,  
52 “ion” means any primary particle with  $Z \geq 1$ . Note, that often the term  
53 Heavy Charged Particles (HCPs) is used, referring to particles with  $Z > 1$ .  
54  
55

56 For a given biological system and chosen endpoint, RBE is a function of the  
57 target parameters, atomic number and velocity of the bombarding particle.  
58 This is why the RBE in the plateau region is different from that in the Bragg-  
59 peak. For protons one generally assumes an RBE close to unity for the entire  
60  
61  
62  
63  
64  
65

1  
2  
3  
4 penetration, even though an increase of RBE beyond this value has been  
5 observed for the distal edge of the Bragg-peak [3, 4].  
6

7  
8 For HCPs the increase of RBE with depth becomes more pronounced and also  
9 shifts towards the entrance to the target with increasing atomic number. For  
10 antiprotons compared to protons of the same energy, the RBE is anticipated  
11 to be further enhanced in the peak region, due to the annihilation process  
12 which yields fragments with  $Z > 1$ . In the plateau region, antiprotons are  
13 expected to exhibit an RBE similar to that of protons.  
14  
15

16  
17 The RE of a detector is expected to behave similar: in the peak region of the  
18 depth-dose curve we expect a lower RE due to secondary particles which may  
19 have a higher LET [5].  
20

21  
22 Attempts to measure the RBE of antiprotons directly in the peak region have  
23 failed so far [6–8], since any RBE determination requires knowledge of the  
24 dose. Dosimetry of the antiproton depth dose curve is problematic since all  
25 applicable dosimeters known to us show non-linear effects in response when  
26 being exposed to ion beams. This is true for e.g. silicon diodes [9, 10], diamond  
27 detectors [10, 11], radiochromic films [12] and alanine [13].  
28  
29

30  
31 At CERN the antiproton beam has a pulsed structure which leads to ionic  
32 recombination effects in ionization chambers [14–17]. Measurements using  
33 Boag’s theorem [18, 19] correcting for recombination effects have been per-  
34 formed and are described in [20]. Calorimetry is the most direct way to measure  
35 absorbed dose according to its definition. However, calorimeters are cumber-  
36 some to use and are not easily applicable in a low-frequency pulsed beam such  
37 as CERN’s antiproton beam. Other detectors we have applied in the antipro-  
38 ton beam are lithium fluoride based thermoluminescent devices (TLDs) and  
39 radiochromic films [21]. This paper, however, will concentrate on the results  
40 achieved with alanine detectors.  
41  
42  
43  
44

45 L- $\alpha$ -alanine is an amino acid which occurs naturally in the human body. When  
46 alanine is irradiated with ionizing radiation, it forms the stable radical  $\text{CH}_3\text{-}$   
47  $\dot{\text{C}}\text{H-COOH}$ . Using an electron spin resonance (ESR) reader, the free electron  
48 pair at the chiral carbon atom can be detected. The magnitude of the ESR  
49 response depends on the amount of absorbed dose, and Bradshaw et al. [22]  
50 first suggested to use this detector as a dosimeter. The behaviour of alanine in  
51 photonic fields is well characterized [23]. The dynamic range of these pellets  
52 is large, ranging from 0.5 Gy to 100 kGy, being linear in the region up to 10  
53 kGy. Kudoh et al. [24] showed that there was no dose rate effect when exposing  
54 2.34 kGy X-rays within 70 ns. The response of alanine detectors to HCPs was  
55 investigated by Hansen and Olsen in the 80’s [25, 26]. A model explaining  
56 the behaviour based upon the Butts and Katz track structure idea [27, 28]  
57 was developed [29]. This model has had some success in predicting the RE of  
58  
59  
60  
61  
62  
63  
64  
65



1  
2  
3  
4 alanine detectors, including fading effects - a phenomenon being of importance  
5 in the evaluation of dose-response for alanine detectors exposed to beams of  
6 HCPs: The temporal instability of the ESR signal in alanine after exposure to  
7 ionizing radiation, has been reported to be rather insignificant at low doses,  
8 but becoming more significant when approaching saturation doses of  $\sim 5 \times 10^5$   
9 Gy [25]. It was measured to be less than 1% per year for low-LET radiation,  
10 but as much as 16% after 4000 hours when exposing alanine to high doses  
11 ( $5 \times 10^5$  Gy) of 16 MeV protons, and 22% for  $10^6$  Gy from stopping 21 MeV  
12  $^7\text{Li}$ -ions [23]. At lower doses (but at the same dose rate), the decay of the ESR  
13 signal from  $10^4$  Gy of 16 MeV protons stabilizes to 3% after 4000 hours. The  
14 decay in alanine is dominant within the first 100 to 200 hours after exposure  
15 to HCPs, and the rate of decay is different for pellets positioned in the plateau  
16 compared to those in the Bragg-peak [30].  
17  
18  
19  
20  
21

22 The difference in fading rate between high and low-LET radiation and high  
23 and low dose is attributed to radical recombination effects in the microscopic  
24 high dose regions of the particle tracks [30]. Fading predictions based on the  
25 model of track structure have shown to conform to experimental data [26].  
26  
27

28 Concluding, due to the higher atomic number of annihilation fragments in the  
29 Bragg-peak of antiprotons the fading processes will be more pronounced and  
30 should from a theoretical point of view be taken into account when comparing  
31 the radiation effect in the Bragg-peak with that of protons.  
32  
33

34 Here we shall apply the track structure model on a mixed particle energy  
35 spectrum simulated by FLUKA, in order to calculate the RE and then the  
36 expected response of alanine pellets based on the measured  $^{60}\text{Co}$   $\gamma$ -ray dose-  
37 response curve. The predicted response as a function of penetration depth is  
38 compared to that measured from a stack of alanine pellets exposed to a beam  
39 of antiprotons.  
40  
41  
42  
43  
44

## 45 2 Experimental Methods

46  
47  
48

49 Two stacks of alanine pellets are irradiated with antiprotons. The pellets in  
50 stack #1 consist of finely grained crystalline alanine powder (Merck) 95% by  
51 weight mixed with 5% by weight polyvinyl-pyrrolidone (Polyvidone, Merck)  
52 as the binding agent and are manufactured by J.W. Hansen. The pellets have  
53 an outer diameter of 4.5 mm, an average thickness of 2 mm, and a density of  
54  $1.210 \text{ g cm}^{-3}$ . Details about the dosimeter pellets are published in [29]. In this  
55 stack seven pellets are placed in the plateau, and 18 pellets are placed around  
56 the annihilation peak and are surrounded by a polystyrene phantom.  
57  
58  
59

60 Stack #2 consists of alanine pellets which are produced by NPL and consists  
61  
62  
63  
64  
65



1  
2  
3  
4 of 90% by weight L- $\alpha$ -alanine and 10% high melting point paraffin wax. The  
5 diameter of the pellets is 5 mm and the thickness is either 2.2 mm or 0.44 mm  
6 (average values for the entire batch). The average density is 1.235 g cm<sup>-3</sup>. The  
7 stack is assembled from eleven 2.2 mm pellets, six 0.44 mm pellets and five  
8 2.2 mm pellets, arranged in a 5.2 mm cylindrical hole in a PMMA phantom.  
9 We used a build-up plate of 81.8 mm polystyrene in order to position the  
10 Bragg-peak around the position of the thin pellets.  
11  
12

13  
14 The Antiproton Decelerator (AD) at CERN provides a 502 MeV/c ( $\sim$ 126  
15 MeV) antiproton beam. Every 90 seconds a spill consisting of roughly  $3 \cdot 10^7$   
16 antiprotons is ejected within 300 ns. The momentum spread of the beam is  
17  $\Delta p/p = 5 \cdot 10^{-4}$ , and the divergence is in the order of 5 mrad. The beam exits  
18 the accelerator vacuum via a thin titanium window and is collimated to 1 cm  
19 diameter.  
20  
21

22  
23 The absolute number of particles extracted from the AD is determined by a  
24 fast current transformer mounted downstream of the extraction septum in the  
25 beam line feeding our experimental set-up. Earlier studies show that this num-  
26 ber possibly has a tendency to overestimate the amount of antiprotons hitting  
27 the target by 10 - 20%. This may be due to calibration errors and/or to losses  
28 in the final stretches of the beam line leading up to our set-up. In addition, for  
29 stack #1 we could only randomly manual check the number of antiprotons per  
30 spill, due to a temporary problem in the AD logging system. Those numbers  
31 were used to derive the best estimate of the amount of antiprotons hitting the  
32 alanine stack. The precision of this estimate is in the order of +/- 5 %. For  
33 stack #2 the problems were solved, and every spill was logged.  
34  
35  
36  
37

38 We verify the alignment of the two stacks with two radiochromic films (GAFChromic  
39 HS and EBT) which are inserted along the beam. The FWHM of the beam  
40 when irradiating stack #2 is almost circular with a FWHM of 0.9 and 1.0  
41 cm along the x and y axis. The beam which is used for stack #1 has a more  
42 ellipsoid form of about 0.6 - 1.0 cm FWHM along the x and y axis, respec-  
43 tively. The ESR signal of the pellets in stack #1 is read out by the Radiation  
44 Research Department at the Risø, National Laboratory in Denmark, using a  
45 Bruker EMS 104 EPR alanine readout device. Stack #1 is read out several  
46 times at increasing time intervals, in order to detect any fading effects, as re-  
47 ported in [30]. At each readout, the pellet is measured at zero and 90° rotation  
48 and a mean signal strength is obtained. Stack #2 is read out at the National  
49 Physics Laboratory (NPL) in the UK using the standard procedures for NPL's  
50 radiotherapy level alanine dosimetry service [31]. The spectrometer is a Bruker  
51 ESX and a standard Bruker ST4102 rectangular cavity. The acquisition time  
52 is 120 s consisting of six 20 s scans with 90° rotation of the pellet between the  
53 third and fourth scan. The pellets are introduced in the spectrometer using  
54 an automated loading system with a specially constructed sample holder to  
55 provide highly accurate positioning [32].  
56  
57  
58  
59  
60  
61  
62  
63  
64  
65

### 3 Model Calculations

FLUKA [33, 34] version 2006.3 is used for calculating the antiproton particle transport through the medium and the distribution of secondaries in each alanine pellet. The geometry of both stacks is carefully implemented, including correct densities and chemical compositions of target and phantom materials. The beam profiles measured with the radiochromic films is used as an input parameter for FLUKA for stack #1 and stack #2. We find for stack #1 a little misalignment of 2 mm and a rotation of the phantom of a half degree, which we include in the FLUKA calculations. 500.000 particles are used for the statistics, using the FLUKA hadron therapy “HADROTHER” default settings. The dose  $D$  for all particles (including contribution from  $\gamma$ -rays) is scored in every pellet position using the “USRBIN” card in FLUKA. A custom user routine is written to determine the dose  $D_\gamma$  from electromagnetic transport ( $\gamma$ -rays, electrons, positrons) and  $D_R$ .  $D_R$  is a dose derived from what FLUKA defines as “kerma energy”, which is energy being transferred to particles which are not transported further and again deposit their energy at the production point. These particles are not further identified in FLUKA, but it is expected to be related to low-energy neutron reactions and possibly also low-energy heavy recoils from the annihilation process.

In addition, we record the track length fluence-energy spectrum  $\phi[E_j, Z_i]$  for pions, kaons and all nuclei with  $1 \leq Z \leq 6$  for each pellet using the “USRTRACK” card in FLUKA. Another user routine is written in order to group all particles of equal charge. For example  $Z = 1$  covers all pions ( $\pi^+$ ,  $\pi^-$ ,  $\pi^0$ ), kaons ( $K^+$ ,  $K^-$ ,  $K_S^0$ ,  $K_L^0$ ,  $K^0$ ,  $\bar{K}^0$ ), antiprotons, protons, deuterons and tritons. Higher charges  $Z \geq 2$  includes all isotopes of the respective charge. The energy binning is done in energy per nucleon, which eases further data processing by using the fact that particles with equal charge and equal energy per nucleon have equal stopping power. For instance, pions are therefore treated as protons with mass  $A = 0.15$  amu. The energy range scored ranges from 10 keV/nucleon to 1 GeV/nucleon in 100 logarithmic steps. We neglect effects of changing the charge sign, since the Barkas effect [35] is insignificant for our calculations. Thus, in all calculations antiprotons have equal stopping power as protons.

From FLUKA we can build a fluence matrix  $\phi[E_j, Z_i]$  which is divided in particle types  $Z_i$  and energy bins with the mean energy per nucleon  $E_j$ .

For the relative efficiency calculations, the same approach of grouping the particles in terms of charge and energy per nucleon is taken, since the default model is not capable of treating pions, antiprotons or kaons.

The track length dose  $D_{TL}$  from these particle-energy spectra can be derived

from  $\phi[E_j, Z_i]$  as:

$$D_{\text{TL}} = \sum_{i=1}^{Z_{\text{proj}}} \sum_{j=1}^{E_{\text{bin}}} \phi[E_j, Z_i] \frac{1}{\rho} \frac{dE}{dx}(E_j, Z_i) \quad (2)$$

where  $\frac{1}{\rho} \frac{dE}{dx}(E_j, Z_i)$  is the mass stopping power for particle  $Z_i$  at energy  $E_j$ . The stopping power is evaluated at the center of the energy bin using the PSTAR and ASTAR routines by Berger et al. [36] for  $Z = 1$  and  $Z = 2$  respectively, and MSTAR (by Paul and Shinner [37, 38]) is used for  $Z > 2$ . Since we use track length dose, the energy dissipation of primary and secondary particles, when passing through the pellet of interest, is accounted for, when calculating  $D_{\text{TL}}$ .

The dose  $D_{\text{TL}}$  calculated by the track length fluence, is lower than the FLUKA dose  $D$ , since photons and low energy recoils are not included in the  $D_{\text{TL}}$  calculation. Instead these contributions are scored directly in  $D_\gamma$  and  $D_{\text{R}}$  as mentioned before. The contribution from  $D_\gamma$  and  $D_{\text{R}}$  to the total dose is about 1-2 % in the plateau region and about 7-9 % in the pellet(s) covering the peak region. The total summed dose  $D_{\text{TOTAL}}$  is therefore

$$D_{\text{TOTAL}} = D_{\text{TL}} + D_\gamma + D_{\text{R}} \quad (3)$$

$D_{\text{TOTAL}}$  still differs from the direct way of calculating the dose  $D$  due to rounding errors from the binning, and perhaps even due to the use of external stopping power tables, which may differ from what FLUKA internally uses. The difference is 4% in the peak and 1% in the plateau.

From the track length fluence matrix  $\phi[E_j, Z_i]$  the relative effectiveness of each particle-energy entry is looked up in a table. This RE table is generated using the model by Hansen and Olsen for infinitesimal thin detectors and the results are shown in figure 1.

By summing all individual detector responses  $R_{\text{ion}}(E_j, Z_i) = \text{RE}(E_j, Z_i)D(E_j, Z_i)$  for each energy bin  $E_j$  and particle type  $Z_i$ , we find a total dose weighted average relative effectiveness  $\overline{\text{RE}}$  of the particle spectrum for the pellet of interest:

$$R_{\text{TL}} = \sum_{i=1}^{Z_{\text{proj}}} \sum_{j=1}^{E_{\text{bin}}} \text{RE}(E_j, Z_i) \phi[E_j, Z_i] \frac{1}{\rho} \frac{dE}{dx}(E_j, Z_i) \quad (4)$$

$$\overline{\text{RE}} = \frac{R_{\text{TL}} + \text{RE}_\gamma D_\gamma + \text{RE}_{\text{R}} D_{\text{R}}}{D_{\text{TOTAL}}} \quad (5)$$

where  $\text{RE}_\gamma$  and  $\text{RE}_{\text{R}}$  is the relative efficiency for the electromagnetic transport and the low-energy recoiling nuclei. Here we set  $\text{RE}_\gamma = 1$  per definition. Since

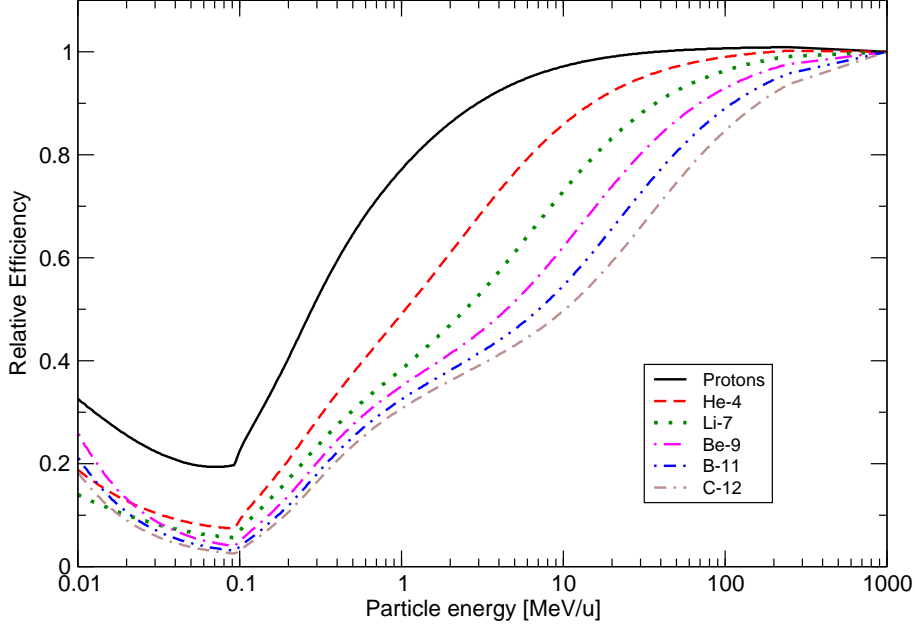


Fig. 1. Calculated relative efficiencies for infinitesimal thin detectors, without fading effects.

FLUKA does not return the exact composition of the low-energy recoils, we cannot calculate  $RE_R$ . Figure 1 indicates that this part the RE may lie between 0.0 and 0.2 for HCPs. since these particles are expected to have energies below 100 keV, which is the default cut-off energy for hadron transport. The Hansen and Olsen model suggest fading effects ranging from 9% to 87% for a  $^{12}\text{C}$  nuclei with 10 keV/nucleon and 100 keV/nucleon, respectively, after 1900 hours of fading. As an estimate we set  $RE_R$  to be = 0.1 with fading, and without fading we set  $RE_R = 0.2$ .

At last, we multiply the calculated  $\overline{RE}$  with the total dose  $D$  (representing the exact dose) scored by FLUKA for each pellet. This gives the response  $R_{\text{ion}}$  expressed in equivalent  $\gamma$ -ray dose:

$$R_{\text{ion}}(D) = \overline{RE} \cdot D \quad (6)$$

## 4 Results

In figures 2 and 3 the total measured response of the alanine pellets as a function of penetration depth is plotted together with the response calculations and the predicted dose for stack #1 and #2, respectively. Fading effects are included in these calculations. The response is expressed in terms of response equivalent gamma dose.

All measurements are absolute, as the total number of antiprotons in the beam

is measured upstream of the target with the beam current transformer. This possibly introduces a systematic error in dose, since fractions of the beam may be lost on the way from the transformer to the experimental setup, as mentioned earlier.

For stack #1 in figure 2 the measured peak was found 1.5 mm further downstream compared to the calculations. Therefore the measurements have been shifted 1.5 mm upstream the beam axis, in order to match the peaks. Investigation of the fading of the alanine tablets is attempted with alanine stack #1. Unfortunately the ESR-spectrometer for these readings turned out to be rather unstable resulting in unreliable measurements for which fading could not be determined with a sufficient accuracy. This error in precision is reflected by the  $1\sigma$  standard deviation error bars in figure 2. From calculated predictions we expect to find a difference of less than 1% in fading between dosimeters positioned at the plateau and in the peak (see also figure 4). Therefore the expected fading is too small to be observable. Most of this fading in response is considered to take place within 200 hours after irradiation. Here we apply 1900 hours of fading for both stacks. As we mentioned earlier it is difficult to assess the amount of fading for  $RE_R$ , since the exact composition is not known.

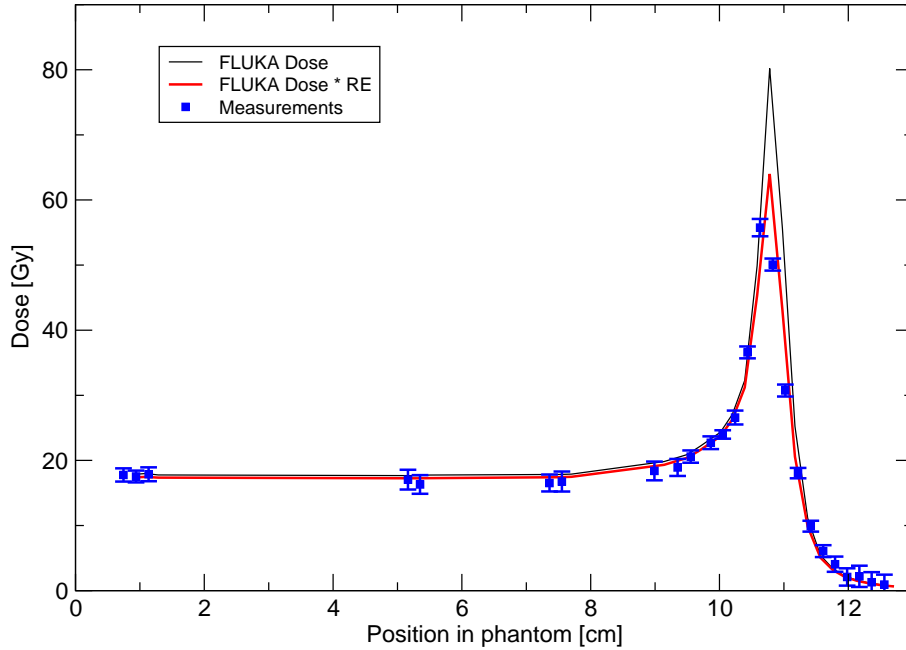


Fig. 2. Stack #1 results. The thin (black) line shows the dose for each pellet as it is calculated by FLUKA. The calculated dose multiplied with the calculated relative effectiveness is plotted as a thick (red) line, and should ideally match the measurements marked as unconnected squares. Measured response is translated to dose using the  $\gamma$ -ray dose-response curve. The measurements are shifted 1.5 mm upstream in order to match the results.

Using equations 4 and 5 the calculated relative effectiveness as a function of

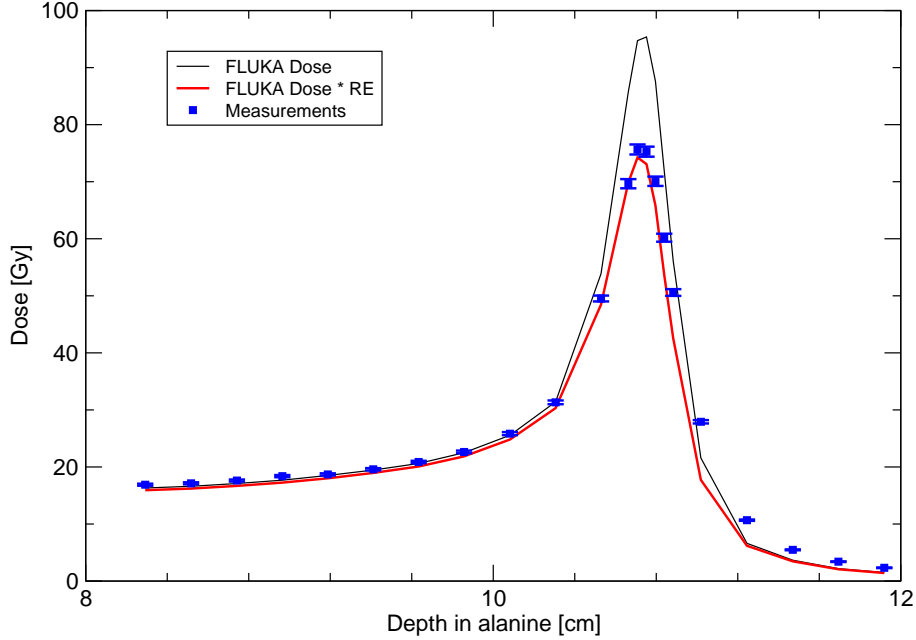


Fig. 3. Results for stack #2 plotted in the same fashion as figure 2. No shift along the x-axis needed to be applied here.

the particle penetration depth for stack #2 is shown in figure 4.

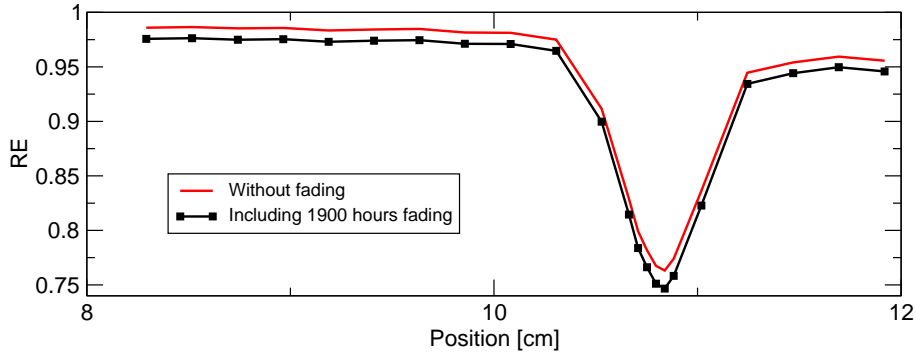


Fig. 4. Calculated relative effectiveness for stack #2 as a function of depth in phantom. The relative effectiveness drops off in the peak region due to the slowing down of antiprotons and the annihilation products with higher LET. The calculation is done twice, including and excluding fading effects.

## 5 Discussion

One of the major differences between stack #1 and #2, is the fitting of the pellet diameter to the  $\varnothing 5$  mm hole drilled into the phantom. Stack #1 leaves a gap in between the pellet and the cavity wall whereas the stack #2 pellets fit the hole exactly. The presence of this gap enables some antiprotons to tunnel past the pellets. Furthermore, the pellets in stack #1 did not have a perfect

1  
2  
3  
4 cylindrical form, but had a little edge at the rim of the outer diameter. These  
5 effects are not included in the FLUKA simulations, since this is difficult to  
6 quantify. The result is that some antiprotons have a larger observed range,  
7 which in turn widens the peak, and localizes it further downstream the beam  
8 axis. This may possibly explain the shift of 1.5 mm downstream from the  
9 predicted position of the measured peak. This effect is thought to be much  
10 less pronounced for stack #2, as these pellets have perfect cylindrical form  
11 which closely matches the phantom cavity.  
12  
13  
14

15  
16 Another difference between both stacks is the density matching of the pellets  
17 and the surrounding phantom. For stack #1 the alanine pellets had  $1.21 \text{ g cm}^{-3}$   
18 and are surrounded by polystyrene with  $1.04 \text{ g cm}^{-3}$ . For stack #2 the  
19  $1.235 \text{ g cm}^{-3}$  pellets are surrounded by a PMMA phantom with a density of  
20  $1.19 \text{ g cm}^{-3}$ . This is accounted for in the FLUKA calculations and causes the  
21 difference in the shape of the tail since antiprotons can penetrate deeper in  
22 the surrounding phantom as in the alanine stack and their annihilation can  
23 contribute to dose beyond the Bragg-peak.  
24  
25  
26

27 The RE is fairly close to unity in the plateau region, and drops down to about  
28 0.75 in the peak region. Compared to the RE of e.g. low energy carbon ions  
29 (see figure 1) the change in RE for antiprotons is rather small. The reason  
30 for this rather slight change in RE is due to the low atomic number of the  
31 antiproton itself but also due to the resulting mixed field of relatively light  
32 nuclei from the antiproton annihilation as described by Polster et al. [39].  
33 Other detectors such as TLDs show a significantly higher loss of RE for light  
34 nuclei with low energy, see e.g. [40, 41].  
35  
36  
37

38 Both stacks provide absolute dose measurements. Since the plateau region of  
39 the stack #2 fits the calculations very well, the systematic effect of a possible  
40 overestimate of the recorded particle fluence due to the upstream position of  
41 the beam current transformer seems to be minor. Absolute dose measurements  
42 for stack #1 are more problematic, since the alanine readout device had a  
43 tendency to drift as mentioned earlier.  
44  
45  
46

47 Due to the volume averaging effects, we focus on the stack #2. Here we see a  
48 6% underestimation of the calculated dose in the plateau region. The agree-  
49 ment of the calculated dose in the annihilation peak is better than 3%, but in  
50 the tail the underestimation is almost  $\sim 40\%$ . The nature of this underestima-  
51 tion is not clear, and several possible explanations exist:  
52  
53  
54

- 55 • unknown accuracy of the beam current monitor
- 56 • incorrect representation of the geometry used as input parameter for the  
57 FLUKA calculations
- 58 • the RE model has shown to be only partially correct for HCP-energies below  
59  $2 \text{ MeV/u}$  [26]
- 60
- 61
- 62
- 63
- 64
- 65



- limitation of the inherent model in the FLUKA code to predict the annihilation peak accurately

On the experimental side a source of error may be the fact that the pellets consists of grains in a matrix whereas the Monte Carlo simulations assume a homogeneous mixture. Finally, the local shape of the annihilation peak is very sensitive to volume averaging effects, which may not be reproduced accurately in the Monte Carlo simulation.

Furthermore it should be noted that alanine together with model calculations of RE is a promising dosimeter in mixed radiation fields as formerly shown for neutrons [42]. In a real clinical situation, one would never use a pristine beam, but a spread out beam covering a larger treatment volume. This dilutes the RE further as the Bragg-peak is mixed with the field from primary particles and reduces the error of dosimetry in the spread out peak region further.

Models based on track structure theory by Butts and Katz [27], and derivatives of the Local Effect Model [43–45] such as ECLaT [46] for TLDs, rely on predicting the response of a detector from the  $\gamma$ -response curve which is convoluted with the radial dose distribution of a track in order to achieve the relative effectiveness of the HCP radiation in question. Here we would like to speculate on the link between track interactions and saturation level of the  $\gamma$ -response curve. In mixed radiation fields, the track structure model and the local effect model use different approaches in calculating track interaction effects, an overview of these differences is given in [47]. In this paper though, the response calculations are further simplified since interactions between two or multiple tracks are not considered. Track interactions are most likely to happen at high fluences where the mean track distance  $\sqrt{\phi^{-1}}$  becomes similar to that part of the track radius in which "cross-overs" would lead to saturation response. For a clinical setting with a fluence of  $10^9 \text{ cm}^{-2}$  (per fraction) the mean track distance would be  $3 \cdot 10^{-5} \text{ cm}$ . One can estimate a significant track-radius from the amorphous radial dose distribution of a track, where saturation effects occur. This radius is depending on particle energy and particle charge, but it will decrease, the higher the onset of saturation is on the  $\gamma$ -response curve. If we assume 10 kGy as the onset of saturation effects for alanine, this would give a radius in the order of  $10^{-6} \text{ cm}$  for an oxygen ion with 3 MeV [30]. This radius will decrease further for decreasing charge. Neglecting of track interactions in the calculation of effectiveness should be possible due to the high saturation dose of alanine.

The region of saturation in a single particle track is smaller in a detector with a high saturation level, i.e. low radiation sensitivity, than that of a detector with a low saturation level, i.e. high radiation sensitivity. Therefore the effect of overlapping tracks is expected to be low for the alanine detector.



## 6 Conclusion

In this paper we have described the use of alanine detectors for the dosimetry of the mixed particle field arising from antiproton annihilation. The results could be reproduced using the relative effectiveness calculated with the track structure model by Hansen and Olsen used in conjunction with doses and particle spectra calculated with FLUKA. Forward calculation using this method shows that dose verification is possible, and in principle medical dosimetry can be reconstructed from the alanine response. We conclude that the alanine detector is an interesting detector for characterizing the mixed radiation field from antiproton annihilation. This detector could also be applied for dosimetry of medical heavy ion beams and possibly in mixed radiation fields found in space. NPL alanine dosimetry service can measure the dose from 5 Gy upwards with a precision of 1% ( $1 \sigma$ ). This is well within the dose levels used in radiotherapy. Even if ESR spectrometers are not widespread in clinical environments and readout may be time-consuming, this dosimeter has still some advantages: it is easy to handle, the read-out is non-destructive, and alanine has a tissue-equivalent composition.

## 7 Acknowledgments

We thank Peter Sharpe and Clare Gouldstone from NPL and Jakob Helt Hansen from Risø, for reading out the alanine dosimeters. We also thank the AD-4 operators for providing us the antiproton beam. The Danish Cancer Society supported this project with a grant.

## References

- [1] L. Gray and T. E. Kalogeropoulos. Possible biomedical applications of antiproton beams: Focused radiation transfer. *Radiation Research*, pages 246–252, 1984.
- [2] A. H. Sullivan. A measurement of the local energy deposition by antiprotons coming to rest in tissue-like material. *Phys. Med. Biol.*, 30(12):1297–1303, 1985.
- [3] Jay S. Loeffler, A. R. Smith, and H. D. Suit. The potential role of proton beams in radiation oncology. *Seminars in Oncology*, 24(6):686–695, 1997.
- [4] B. G. Wouters, G. K. Y. Lam, U. Oelfke, K. Gardey, R. E. Durand, and L. D. Skarsgard. Measurements of relative biological effectiveness of the 70 MeV proton beam at TRIUMF using chinese hamster V79 cells and the high-precision cell sorter assay. *Radiation Research*, 146(2):159–170, 1996.

- 1  
2  
3  
4 [5] K. J. Olsen and J. W. Hansen. Experimental and calculated effectiveness of a  
5 radiochromic dye film to stopping 21 MeV  ${}^7\text{Li}$  and 64 MeV  ${}^{16}\text{O}$  ions. *NIM B*,  
6 5:497–504, 1984.  
7  
8  
9 [6] Michael H. Holzscheiter, Nzhde Agazarayan, Niels Bassler, Gerd Beyer, John J.  
10 DeMarco, Michael Doser, Toshiyasu Ichioka, Keisuke S. Iwamoto, Helge V.  
11 Knudsen, Rolf Landua, Carl Maggiore, William H. McBride, Søren Pape Møller,  
12 Jorgen Petersen, James B. Smathers, Lloyd D. Skarsgard, Timothy D. Solberg,  
13 Ulrik I. Uggerhøj, H. Rodney Withers, Sanja Vranjes, Michelle Wong, and  
14 Bradly G. Wouters. Biological effectiveness of antiproton annihilation. *NIM*  
15 *B*, 221:210–214, 2004.  
16  
17  
18 [7] Carl Maggiore, Nzhde Agazarayan, Niels Bassler, Ewart Blackmore, Gerd  
19 Beyer, John J. DeMarco, Michael Doser, Charles R. Gruhn, Michael H.  
20 Holzscheiter, Toshiyasu Ichioka, Keisuke S. Iwamoto, Helge V. Knudsen,  
21 Rolf Landua, William H. McBride, Søren Pape Møller, Jorgen Petersen,  
22 James B. Smathers, Lloyd D. Skarsgard, Timothy D. Solberg, Ulrik I. Uggerhøj,  
23 H. Rodney Withers, and Bradly G. Wouters. Biological effectiveness of  
24 antiproton annihilation. *NIM B*, 214:181–185, 2004.  
25  
26  
27 [8] Michael H. Holzscheiter, Niels Bassler, Nzhde Agazaryan, Gerd Beyer, Ewart  
28 Blackmore, John J. DeMarco, Michael Doser, Ralph E. Durand, Oliver  
29 Hartley, Keisuke S. Iwamoto, Helge V. Knudsen, Rolf Landua, Carl Maggiore,  
30 William H. McBride, Søren Pape Møller, Jørgen Petersen, Lloyd D. Skarsgard,  
31 James B. Smathers, Timothy D. Solberg, Ulrik I. Uggerhøj, Sanja Vranjes,  
32 H. Rodney Withers, Michelle Wong, and Bradly G. Wouters. The biological  
33 effectiveness of antiproton irradiation. *Radiotherapy and Oncology*, 81(3):233–  
34 242, December 2006.  
35  
36  
37 [9] E. Grusell and J. Medin. General characteristics of the use of silicon diode  
38 detectors for clinical dosimetry in proton beams. *Phys Med Biol.*, 45(9):2573–  
39 2582, 2000.  
40  
41  
42 [10] S. Onori, C. De Angelis, P. Fattibene, M. Pacilio, E. Petetti, L. Azario, R. Miceli,  
43 A. Piermattei, L. Barone Tonghi, G. Cuttone, and S. Lo Nigro. Dosimetric  
44 characterization of silicon and diamond detectors in low-energy proton beams.  
45 *Phys. Med. Biol.*, 45:3045–3058, 2000.  
46  
47  
48 [11] Makoto Sakama, Tatsuaki Kanai, Yuki Kase, Masataka Komori, Akifumi  
49 Fukumura, and Toshiyuki Kohno. Responses of a diamond detector to high-  
50 LET charged particles. *Phys. Med. Biol.*, 50:2275–2289, 2005.  
51  
52  
53 [12] A. Piermattei, R. Miceli, L. Azario, A. Fidanzio, S. delle Canne, C. De Angelis,  
54 S. Onori, M. Pacilio, E. Petetti, L. Raffaele, and M. G. Sabini. Radiochromic  
55 film dosimetry of a low energy proton beam. *Medical Physics*, 27(7):1655–1660,  
56 2000.  
57  
58 [13] H. Palmans. Effect of alanine energy response and phantom material on depth  
59 dose measurements in ocular protons beams. *Technology in Cancer Research &*  
60 *Treatment*, 2(6):579–586, 2003.  
61  
62  
63  
64  
65

- 1  
2  
3  
4 [14] Frank H. Attix. *Introduction to Radiological Physics and Radiation Dosimetry*.  
5 John Wiley & Sons, 1986.  
6  
7 [15] Tatsuoaki Kanai, Michio Sudo, Naruhiro Matsufuji, and Yasuyuki Futami. Initial  
8 recombination in a parallel-plate ionization chamber exposed to heavy ions.  
9 *Phys. Med. Biol.*, 43:3549–3558, 1998.  
10  
11 [16] Hugo Palmans, Russel Thomas, and Andrzej Kacperek. Ion recombination  
12 correction in the clatterbridge centre of oncology clinical proton beam. *Phys.*  
13 *Med. Biol.*, 51:903–917, 2006.  
14  
15 [17] S. H. Park, Y. K. Kim, H. S. Kim, S. M. Kang, and J. H. Ha. Characteristics  
16 of the saturation curve of the ionization chambers in overlapping pulsed beams.  
17 *NIM A*, 566:706–712, 2006.  
18  
19 [18] J. W. Boag and J. Curren. Current collection and ionic recombination in small  
20 cylindrical ionization chambers exposed to pulsed radiation. *British Journal of*  
21 *Radiology*, 53:471–478, 1980.  
22  
23 [19] J. W. Boag, E. Hochhäuser, and O. A. Balk. The effect of free-electron collection  
24 on the recombination correction to ionization measurements of pulsed radiation.  
25 *Phys. Med. Biol.*, 41:885–897, 1996.  
26  
27 [20] N. Bassler, M. H. Holzscheiter, O. Jäkel, S. Kovacevic, H. V. Knudsen, and the  
28 AD-4/ACE Collaboration. The antiproton depth-dose curve in water. [*accepted,*  
29 *not in press yet*] *Phys. Med. Biol.*, 2008.  
30  
31 [21] Niels Bassler. *Experimental Studies Relevant for Antiproton Cancer Therapy*.  
32 PhD thesis, Aarhus University, May 2006.  
33  
34 [22] W. W. Bradshaw, D. Cadena, G. W. Crawford, and H. A. W. Soetzel. The  
35 use of alanine as a solid dosimeter. *Radiation Research*, 17:11–21, 1962.  
36  
37 [23] J. W. Hansen, K. J. Olsen, and M. Wille. The alanine radiation detector for  
38 high and low LET dosimetry. *Radiation Protection Dosimetry*, 19(1):43–47,  
39 1987.  
40  
41 [24] H. Kuhdoh, M. Celina, R. J. Kaye, K. T. Gillen, and R. L. Clough. Response  
42 of alanine dosimeters at very high dose rate. *Appl. Radiat. Isot.*, 48(4):497–499,  
43 1997.  
44  
45 [25] J. W. Hansen and K. J. Olsen. Theoretical and experimental radiation  
46 effectiveness of the free radical dosimeter alanine to irradiation with heavy  
47 charged particles. *Radiation Research*, 104:15–27, 1985.  
48  
49 [26] K. J. Olsen and J. W. Hansen. The response of the alanine dosimeter to low  
50 energy protons and high energy heavy charged particles. *Radiation Protection*  
51 *Dosimetry*, 31(1/4):81–84, 1990.  
52  
53 [27] J. J. Butts and Robert Katz. Theory of RBE for heavy ion bombardment of  
54 dry enzymes and viruses. *Radiation Research*, 30:855–871, 1967.  
55  
56  
57  
58  
59  
60  
61  
62  
63  
64  
65

- 1  
2  
3  
4 [28] R. Katz, S. C. Sharma, and M. Homayoonfar. The structure of particle tracks.  
5 In F. H. Attix, editor, *Topics of Radiation Dosimetry*, volume Suppl. 1, pages  
6 317–383. New York Academic Press, 1972.  
7  
8  
9 [29] J. W. Hansen. *Experimental Investigation of the Suitability of the Track  
10 Structure Theory in Describing the Relative Effectiveness of High-LET  
11 Irradiation of Physical Radiation Detectors*. PhD thesis, Risø National  
12 Laboratory, DK-4000 Roskilde, 1984. Risø-R-507.  
13  
14 [30] J. W. Hansen and K. J. Olsen. Predicting decay in free-radical concentration  
15 in L- $\alpha$ -Alanine following high-LET radiation exposures. *Appl. Radiat. Isot.*,  
16 40(10-12):935–939, 1989.  
17  
18 [31] P. H. Sharpe, K. Rajendran, and J. P. Sephton. Progress towards an  
19 alanine/ESR therapy level reference dosimetry service at NPL. *Appl Radiat  
20 Isot.*, 47(11-12):1171–5, Nov-Dec 1996.  
21  
22 [32] P. Sharpe and J. Sephton. An automated system for the measurement of  
23 alanine/EPR dosimeters. *Appl Radiat Isot.*, 52(5):1185–8, May 2000.  
24  
25 [33] A. Fassò, A. Ferrari, J. Ranft, and P. R. Sala. FLUKA: a multi-particle  
26 transport code. CERN-2005-10, INFN/TC\_05/11, SLAC-R-773.  
27  
28 [34] *The physics models of FLUKA: status and recent developments*, La Jolla,  
29 CA, USA, March 24-28 2003. (paper MOMT005), eConf C0303241 (2003),  
30 arXiv:hep-ph/0306267.  
31  
32 [35] S. P. Møller, A. Csete, T. Ichioka, H. Knudsen, U. I. Uggerhøj, and H. H.  
33 Andersen. Antiprotons stopping at low energies: Confirmation of velocity-  
34 proportional stopping power. *Physical Review Letters*, 88(19):193201–1, 2002.  
35  
36 [36] M. J. Berger, J. S. Coursey, M. A. Zucker, and J. Chang. Stopping-power and  
37 range tables for electrons, protons, and helium ions.  
38 <http://physics.nist.gov/PhysRefData/Star/Text/contents.html>.  
39  
40 [37] H. Paul and A. Schinner. MSTAR.  
41 <http://www.exphys.uni-linz.ac.at/stopping/>.  
42  
43 [38] H. Paul and A. Schinner. An empirical approach to the stopping power of solids  
44 and gases for ions from  $^3\text{Li}$  to  $^{18}\text{Ar}$ . *NIM B*, 179:299, 2001.  
45  
46 [39] D. Polster, D. Hilscher, H. Rossner, T. von Egidy, F. J. Hartmann, J. Hoffmann,  
47 W. Schmid, I. A. Pshenichnov, A. S. Iljinov, Ye. S. Golubeva, H. Machner, H. S.  
48 Plendl, A. Grouchulska, J. Jastrzebski, W. Kurcewiz, P. Lubinski, J. Eades, and  
49 S. Neumaier. Light particle emission induced by stopped antiprotons in nuclei:  
50 Energy dissipation and neutron-to-proton ratio. *Physical Review C*, 51(3):1167–  
51 1180, 1995.  
52  
53 [40] J. Besserer, P. Bilski., J. de Boer., T. Kwiecien, M. Moosburger, P. Olko, and  
54 P. Quicken. Dosimetry of low-energy protons and light ions. *Phys. Med. Biol.*,  
55 46:473–485, 2001.  
56  
57  
58  
59  
60  
61  
62  
63  
64  
65

- 1  
2  
3  
4 [41] J. Kalef-Ezra and Y. S. Horowitz. Heavy charged particle thermoluminescence  
5 dosimetry: Track structure theory and experiments. *Int. J. Appl. Radiat. Isot.*,  
6 33:1085–1100, 1982.  
7  
8 [42] H. M. Gerstenberg, J. W. Hansen, J. J. Coyne, and J. Zoetelief. Calculations of  
9 the relative effectiveness of alanine for neutrons with energies up to 17.1 MeV.  
10 *Radiation Protection Dosimetry*, 31(1/4):85–89, 1990.  
11  
12 [43] M. Scholz. Grundlagen der biologischen Bestrahlungsplanung für die  
13 Schwerionen-Tumorthherapie. Medizinische Fakultät Heidelberg, Ruprecht-  
14 Karls-Universität. Habilitationsschrift. (In German).  
15  
16 [44] M. Scholz and G. Kraft. Track structure and the calculation of biological effects  
17 of heavy charged particles. *Adv. Space Res.*, 18(1/2):(1/2)5–(1/2)14, 1995.  
18  
19 [45] M. Scholz, A. M. Kellerer, and W. Kraft-Weyrather. Computation of cell  
20 survival in heavy ion beams for therapy. *Radiat. Environ. Biophys.*, 36:59–66,  
21 1997.  
22  
23 [46] O. B. Geiß, M. Krämer, and G. Kraft. Efficiency of thermoluminescent detectors  
24 to heavy charged particles. *NIM B*, 142:592–598, 1998.  
25  
26 [47] H. Paganetti and M. Goitein. Biophysical modelling of proton radiation effects  
27 based on amorphous track models. *Int. J. Radiat. Biol.*, 77(9):911–928, 2001.  
28  
29  
30  
31  
32  
33  
34  
35  
36  
37  
38  
39  
40  
41  
42  
43  
44  
45  
46  
47  
48  
49  
50  
51  
52  
53  
54  
55  
56  
57  
58  
59  
60  
61  
62  
63  
64  
65

## **Appendix D: Current list of Collaborators in AD-4**

**Aarhus University, Dept. of Phys. & Astronomy, DK-Aarhus C, Denmark**  
Helge KNUDSEN, Søren PAPE-MØLLER, Ulrik UGGERHØJ

**Aarhus University Hospital , Nørrebrogade 44, DK-8000 Aarhus, Denmark**  
Jan ALSNER, Niels BASSLER, Jens OVERGAARD, Jørgen PETERSEN, Brita SØRENSEN-SINGERS

**CERN, Division EP, CH-1211 Geneva, Switzerland**  
Michael DOSER

**David Geffen School of Medicine at UCLA, Los Angeles, CA 90095, USA**  
John J. DeMARCO, Keisuke S. IWAMOTO, William H. McBRIDE

**Deutsches Krebsforschungszentrum (DKFZ), 69120 Heidelberg, Germany**  
Niels BASSLER, Oliver JÄKEL

**Geneva University Hospital, 1 rue Michel Servet, CH-1211 Geneva, Switzerland**  
Gerd BEYER, Oliver HARTLEY, Osman RATIB, Raymond MIRALBELL

**Queen's University Belfast, Belfast BT7 1NN, UK**  
Adam HUNNIFORD, Robert MCCULLOUGH

**University of Athens, 157 71 Athens, Greece**  
Angelo ANGELOPOULOS, Ioannis KANTEMIRIS

**University of Maastricht, Res. Inst. Growth and Development, The Netherlands**  
Bradly G. WOUTERS

**University of Montenegro, Nikca od Rovina 53, Podgorica, Montenegro**  
Dragan HAJDUKOVIC, Sandra KOVACEVIC

**University of Nebraska Medical Center, Omaha, NE 68198, USA**  
Timothy SOLBERG

**University of New Mexico, Dept. of Phys. & Astr., Albuquerque, NM 87131, USA**  
Michael H. HOLZSCHEITER

**Vinca Institute of Nuclear Sciences, 1101 Belgrade, Serbia & Montenegro**  
Sanja VRANJES